SURE 静岡大学学術リポジトリ
Shizuoka University REpository

Laser trapping for measuring viscosities of liquids and mechanical properties of the biological cells

メタデータ	言語: en 出版者: Shizuoka University 公開日: 2017-12-14 キーワード (Ja): キーワード (En): 作成者: Statsenko, Anna メールアドレス: 所属:
URL	https://doi.org/10.14945/00024354

静岡大学博士論文

Laser trapping for measuring viscosities of liquids and mechanical properties of the biological cells
レーザートラッピングを用いた液体の粘性測定および細部の機械的特性の測定に関する研究

Statsenko Anna

大学院自然科学系教育部

ナノビジョン工学専攻

2017 年 6 月

Dedicated to

Рідному татові

Chapter 1

Introduction

Chapter 2

Applications of laser trapping

Chapter 3

The theory of laser trapping

Chapter 4

Experimental optical setup for laser trapping

Chapter 5

Laser trapping parameters

Chapter 6

The method for measuring viscosity of liquids using laser trapping technique

Chapter 7

Applying laser trapping technique for measuring mechanical properties of the biological cells

Chapter 8

Chapter 1

Introduction

1.1 Pressure of light and first optical traps

Lebedev measured a pressure of light for the first time in 1899. He proved experimentally that light pressures both on reflecting and on absorbing surfaces with the force proportional to the energy of the beam [1].

Ashkin is a pioneer in optical trapping. In 1970s, trapped and levitated liquid drops by radiation pressure, based on the ability of light to trap nanoabsorbing particles [2]. Figure 1.1 shows the experimental setup for trapping and levitation of the drops. From Figure 1.2, one can see the levitated drops, they arrange themselves depending on the size. The largest drops are the closest to the beam focus.

The levitated 1-40-μm drops were made from different liquids in order to reduce evaporation and to increase the time of holding in the trap. The argon ion laser operating at 514.5 nm was used, and operating at 400mW for trapping 35-μ particle and 0.2mW for 1-μm particles. As a next step, they report about trapping and manipulation of viruses and bacteria [3]. The trapping of individual tobacco mosaic viruses and motile bacteria was demonstrated. The bacteria or virus was trapped and manipulated while being viewed under optical microscope. First, the Brownian motion of viruses and bacteria was observed and before an object was trapped and manipulated at the laser power of 100-300mW. A sudden increase in a scattered light

was observed when a virus was trapped. At the point perpendicular to the laser beam, the scattered light was detected.

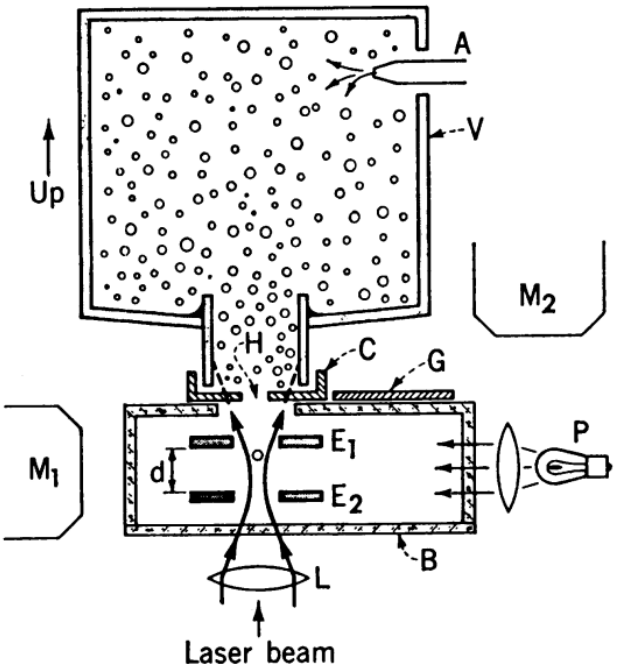

Figure 1.1. Schematic of the experimental apparatus. Dimension *d* is ~0.6 cm. L-lens, B-glass box, H-hole about 0.5 mm in diameter, C- sliding roof cover, V– large storage vessel, A- atomizer, M_1- microscope, E_1, E_2- two plane electrodes with a narrow slit, which allows the beam to pass through, G-sliding glass plate. M_2- microscope for viewing from above [2].

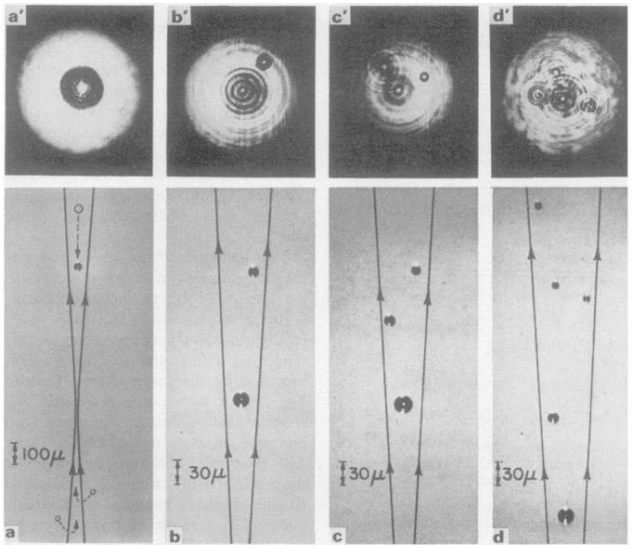

Figure 1.2 Photos of optically levitated drops. (a-d) Side views taken with microscope M_1. (a'-d') Corresponding top views taken with microscope M_2; (a'-c') focus on the highest drop, and (d') focuses lower in the beam, showing the diffraction rings from the four lowest drops [2].

To trap bacteria, initially 50mW of laser power was used, and then the laser power was reduced to 5mW in order not to damage the trapped bacteria. The bacteria were killed at 100mW and the remains of it could be held in the trap with laser power as low as 0.5mW. At powers 3-6mW they were able to catch a lot of bacteria within the trap. Bacteria captured with powers in the range 1-6mW stayed trapped for hours without any damage, but for powers of 100mW or more, it was possible to observe shrinkage of the bacteria. For these experiments, the argon laser with the wavelength of 514.5 nm was used and in order to avoid damage of the samples, Arthur Ashbin propose to use other laser wavelengths. Next, infrared laser traps for trapping biological cells and manipulation organelles within single cells were developed [4]. The E. coli bacteria lose mobility soon while being trapped at the visible laser wavelength. It was found that trapping with infrared laser at the wavelength 1064 nm gave an ability of trapping E. coli bacteria for a total of 5hr during which time they went through 2 ½ life cycles with all progeny staying in the trap. Not only E. coli bacteria shows good characteristics while being trapped by infrared, but also others cells, like Yeast cells (Figure 1.3) were reproduced. Red blood cells and plant cells were strongly damaged by green laser, but not while trapped with infrared light. Proteins have absorption maximum in UV region and as the wavelength increases the absorption decreases.

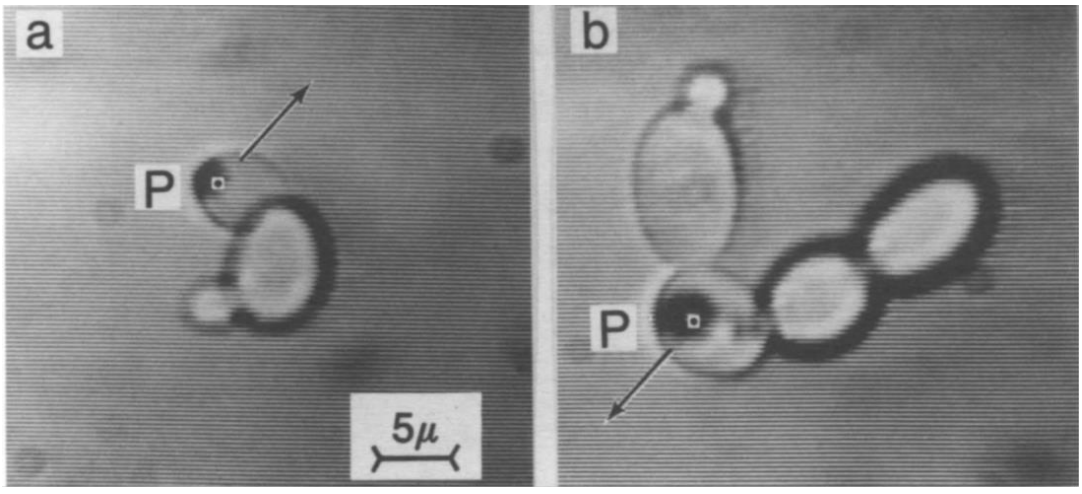

Figure 1.3 Yeast cells survive in the trap long enough to bud and produce progeny. The micro colony is held in place by an optical trap focused at the point “P.”

1.2 Observation of optically trapped atoms

The smallest particle to be trapped was atom. Steven Chu and others including A. Ashkin reported about experimental observation of optically trapped atoms by the force of resonance-radiation pressure in 1986. Optical traps of atoms are difficult to achieve because their potential wells are shallow, their volumes are quite small, after being trapped atoms are heated by the random fluctuations of the light forces and will “boil” out of the trap in a fraction of a second [5]. Optical molasses (OM) was used for cooling the sodium atoms. The observation of trapped atoms was provided by video camera. Figure 1.4 (a) demonstrates the fluorescence from atoms in the initial showing beam, the subsequently formed OM cloud and atoms collecting in the trap. Figure 1.4 (b) shows the bright spot from the trapped atoms which remain in the trap after most of the surroundings cloud of cold atoms.

They provided several tests for confirmation of the trapping. First of all, the bright oval-shaped spot coming from trapped atoms occurs only for tuning within the range expected for axial trapping, which was calculated previously. As a next test, they observed visually that the life time of trapped atoms was longer than for confined OM atoms. The shape of the trap fluorescence varied with tuning the trap-laser intensity as expected from the calculated axial potential profiles. It was concluded that the best trap signals were due to about 500 atoms. And that the collection of trapped atom could be easily moved at speeds on order of 1 cm/s by manually scanning the location of the trap focal spot. So, the optical trapping was experimentally observed and is in good agreement with theoretical calculations.

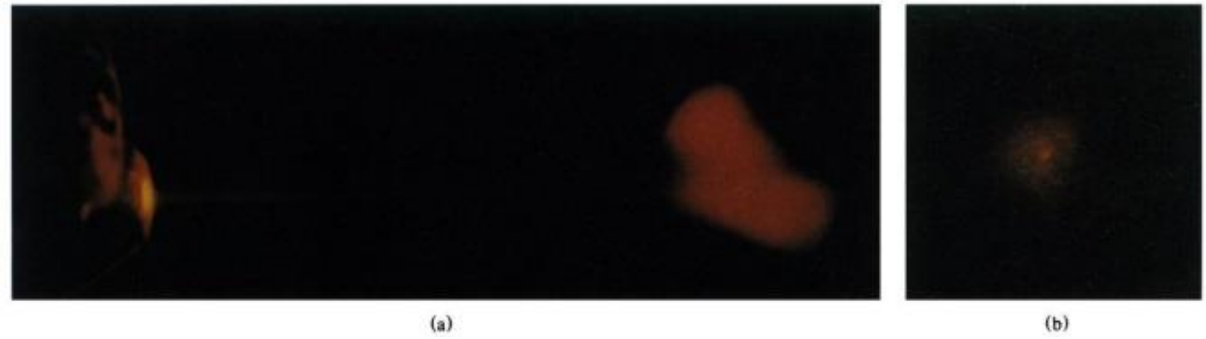

Figure 1.4 (a) Photo showing the collimating nozzle, atomic beam, and atoms confined in OM. The distance from the nozzle to the OM region is 5 cm. (b) Photo taken after the atomic source and the slowing laser beam have been turned off, showing trapped atoms [5].

1.3 Trapping of nanoparticles

The nanoparticles are considered to be trapped in Rayleigh regime as the diameter of the particles are much smaller compare to the ordinary NIR lasers used for trapping. In this case, the mechanism of trapping is explained by considering the nanoparticle as an induced point dipole moving in an inhomogeneous electromagnetic field. The trapped particle is affected by the gradient and radiation force [7]:

$$\boldsymbol{F_{grad}} = \frac{\mathbf{1}}{\mathbf{2}}|\boldsymbol{\alpha}|\boldsymbol{\nabla}\langle \boldsymbol{E^2}\rangle \tag{1.3.1}$$

$$\boldsymbol{F_{rad}} = \frac{\boldsymbol{n}*\boldsymbol{<P>}}{\boldsymbol{c}}\boldsymbol{C_{ext}} \tag{1.3.2}$$

E is the electromagnetic field, ***α*** is the polarizability of the particle, **<P>** the time average of the Poynting vector.

C_{ext} is the extinction cross section which is a sum of the absorption and scattering cross sections:

$$C_{ext}=C_{scat} + C_{abs}= \frac{k^4|\alpha|^2}{4\pi} + k\alpha'' \tag{1.3.3}$$

k is the wave number, $k = 2\pi n/\lambda$, α'' denotes the imaginary part of the polarizability, ε_m dielectric permittivity of the medium

ε_p dielectric permittivity of the particle at the appropriate wavelength.

A critical factor for optical trapping is the particle material, polarizability *α:*

$$\alpha = 3V \frac{\varepsilon_p - \varepsilon_m}{\varepsilon_p + 2\varepsilon_m} \ , \ (d \ << \lambda) \qquad (1.3.4)$$

The particle polarizability, *α* is wavelength dependent and can exhibit a resonance in the optical or NIR spectrum. Therefore, the gradient force, the radiation force, and the particle absorption change dramatically across such a resonance [7]. In the following, trapping at resonance will refer to trapping using a wavelength overlapping with the peak polarizability, whereas off-resonant trapping refers to trapping using a wavelength which is several hundred nanometers away from the peak [8]. Plasmon resonances in metallic particles are due to resonant field induced oscillations of the conduction electrons. At resonance, absorption and scattering are strongly enhanced [9]. Silica and polystyrene are used among dielectric materials. These materials have higher refraction indexes than that of the water, which is an important condition for achieving stable trapping. The trapping force increases linearly with particle size up to the 1 micron at which the particle size starts to exceed the size of focal spot. The Figure 1.6 shows how the force depends on the size of the trapped polymer sphere. The strongest trapping was achieved for the polymer sphere with diameter closed to the size of the trapping wavelength.

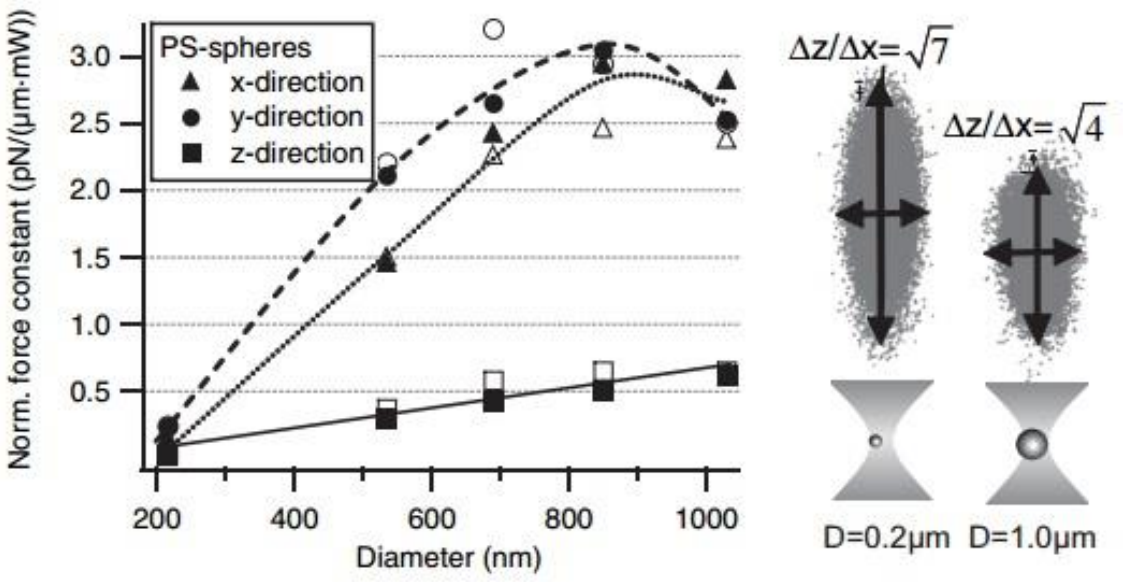

Figure 1.6. Change of the force constant per unit laser power for various polystyrene spheres (λ= 800 nm in water). White markers indicate theoretical values, black markers experimentally obtained stiffnesses, experimental error bars are all below 1% [10].

Metallic objects reflect light and have been considered as poor candidates for laser trapping, Karel Svoboda and Steven Block demonstrated that stable trapping can occur with optical tweezers when they are used with small metallic Rayleigh particles [6]. They show that the trapping of metallic is possible in the Rayleigh regime when the radius of the trapped particle is much smaller than the wavelength of the trapping laser. The trapping forces for 36 nm diameter gold particles and 38-nm-diamater latex particles were compared. In addition, it was shown that the ratio of trapping forces equal the ratio of polarizabilities. For gold particles, the trapping was stronger by the factor of seven than for polymer spheres. The trapping of 36-nm particles was possible for the laser powers above 100mW, if the laser power was below 100mW the particles were trapped only for 5 secs before escaping the trap. Higher powers were required for 38-nm latex particles.

The trapping of gold nanoparticles as small as 9 nm is possible if the spherical aberration can be overcome. Spherical aberrations are present in all focus spots; therefore, it was proposed special immersion oils for minimizing the aberration [11]. Figure 1.7 shows the spring constant for trapped golden nanoparticles with various sizes.

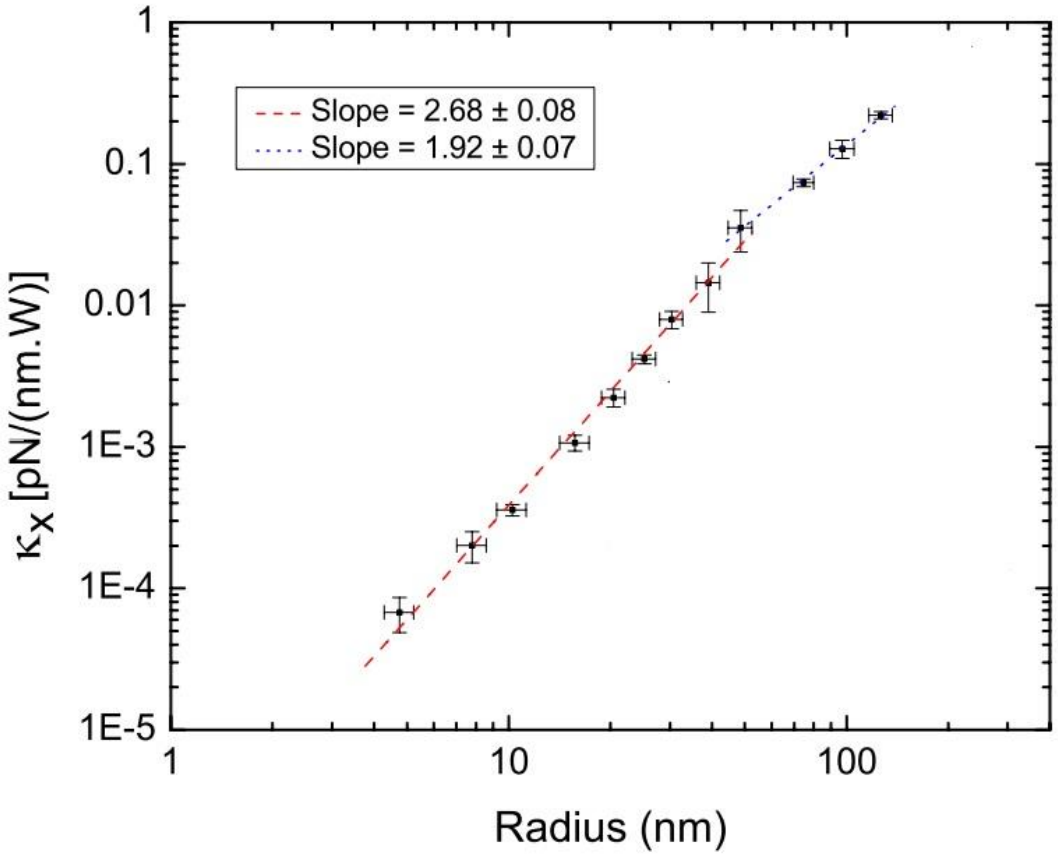

Figure 1.7 Spring constants characterizing the lateral strength of the optical trap while trapping gold nanoparticles of various sizes [12].

Metallic nanorods are extremely interesting for biological applications, due to their tunable resonance across visible and NIR spectrum and orientation depending on heating properties. If one can rotate the polarization of the trapping laser beam, the tapped nanorod will rotate in order to be aligned with the polarization of the trapping laser beam. Optical setup for trapping nanorods and alignment nanorods following laser polarization is shown in Figure 1.8. The various nanorods with diameter down to 8 nm were used for trapping, the overview of the samples is presented in Table 1.

The observation of nanorod trapping was confirmed using power spectra, from the Figure 1.9 you can see how the spectrum of trapped and not trapped particles differs. From measurement of power spectrum one can understand if the particle is trapped and the trapping force can be obtained. The power spectrum differs for different sizes of nanorods as the trapping force is different for different sizes of nanorods. This figure shows that the trapping of 85 nm nanorods is stonger than the trapping of 41 nm nanorods. Also, we can see how the spectrum looks like when the there is no particle in the trap (grey line). The spectrum was taken online while performing an

experiment. This Figure also compares the trapping of different sizes of nanorods. By checking position distribution of the trapped nanorod, it was possible to distinguish if a single nanorod is trapped or not. The histogram broadens as the number of trapped rods increases.

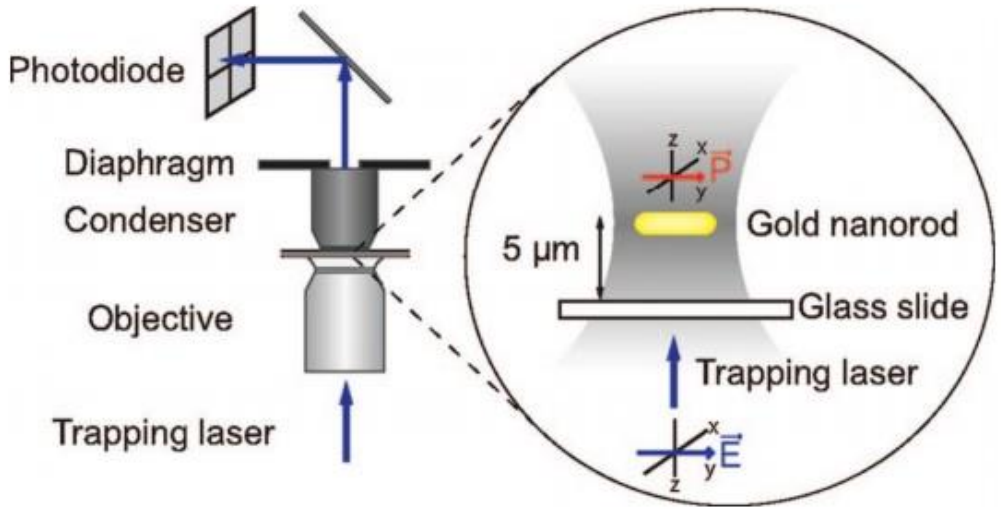

Figure 1.8. Illustration of the optical tweezers, the detection system, and the gold nanorod in the trap. E is the electric field vector of the laser, P is the direction of polarization [13].

Table 1. Overview of gold nanorod samples used for optical trapping.

diameter (nm)	length (nm)	aspect ratio	λ (nm)
8.3 ± 1	41.2 ± 8.3	5.0	876
8.4 ± 1	47.3 ± 8.3	5.6	963
13.1 ± 2.2	22.7 ± 5	1.7	750
12.1 ± 2.5	35.7 ± 8.7	3.0	782
10.7 ± 1.6	51.9 ± 7.6	4.9	909
12.8 ± 2.5	41.5 ± 5.5	3.2	732
13.8 ± 1.6	55.0 ± 7.8	4.0	799
13.3 ± 1.9	59.3 ± 11.2	4.5	899
13.1 ± 1.8	63.8 ± 10.4	4.9	871
21.5 ± 5.9	46.6 ± 6.2	2.2	643
19.4 ± 2.5	56.9 ± 4.7	2.9	696
24.4 ± 4.5	57.9 ± 7.3	2.4	648
27.1 ± 4.3	59.9 ± 6.5	2.2	644
30.1 ± 4.7	56.9 ± 5.0	1.9	608
36.5 ± 5.4	64.2 ± 13.3	1.8	614
37.3 ± 5.0	63.8 ± 7.4	1.7	602
36.8 ± 7.9	69.4 ± 8.1	1.9	611
44.1 ± 6.5	85.1 ± 7.3	1.9	632

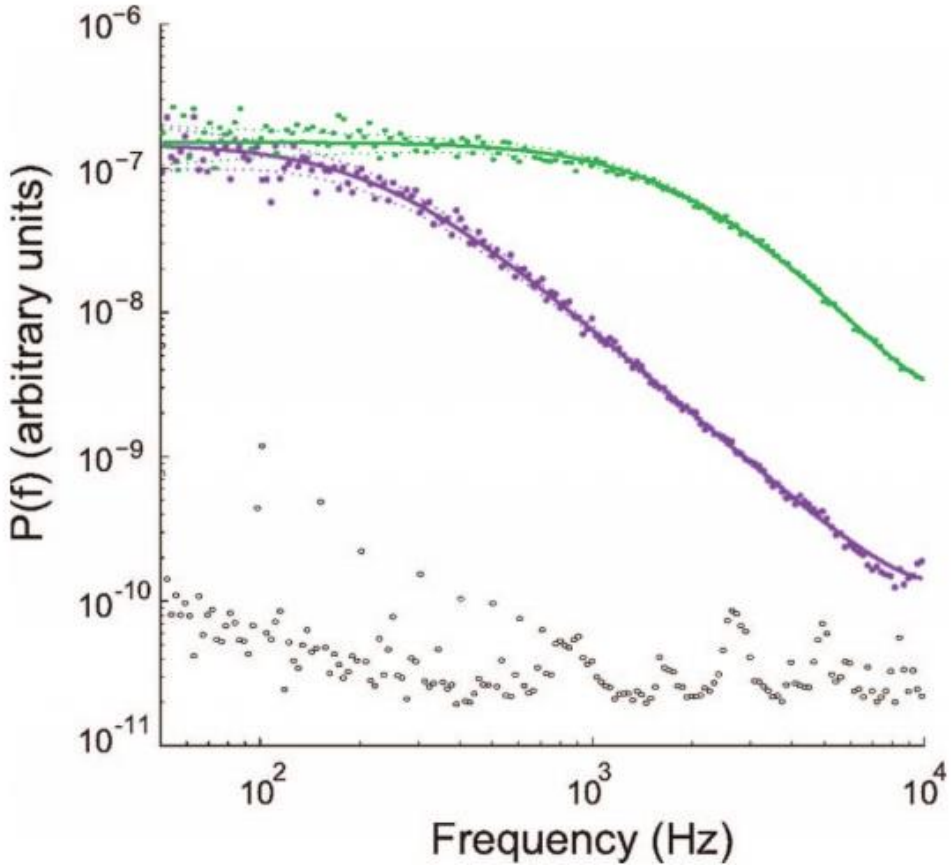

Figure 1.9. Power spectra for gold nanorods with length 85.1 (7.3 nm and width 44.1 (6.5 nm (green) and length 41.2 (8.3 nm and width 8.3 (1 nm (purple) at a laser power of 115 mW at the sample. The fits to the data are given by the full lines. Black circles show the power spectrum for an empty trap [13].

It was reported, that trapping of gold nanorods can be used as efficient optical trapping handles in nanoscale experiments; as force sensors for vivo studies, force transducers in single molecular measurements, nanorotators [13].

Quantum dots are widely used in biology for labeling single proteins and cellular organelles. Colloidal quantum dots are fluorescent semiconductor nanocrystals, which have extremely bright and narrow emission spectrum. The excitation spectrum is quite broad and the emission wavelength depends on the size of quantum dot. These characteristics make quantum dots as excellent markers to visualize biological systems. It was reported that optical trapping of individual quantum dots using CW infrared laser operated at only 0.5 W was possible [14]. Only 20% of applied laser power reached sample. As it's important to trap a single quantum dot, very low concentration of quantum dots was used. To confirm if a single quantum dots in trap,

the experiment to visualize the fluorescence blinking of a trapped quantum dot had to be performed. However, the quantum dots perform a Brownian motion within the trap it is difficult to find out the nature of observed blinking, which can be caused by leaving or entering the focal volume by quantum dot. Therefore, they trapped streptavidin-coated quantum dots and moved to a biotinylated surface, where it would bind especially. Figure 1.10 shows the picture of the coverslip surface before the quantum dots was attached (a) and after the trap with the quantum dots has been lowered and the quantum dots has attached to the surface (b). Finally, a blinking behavior that proves that a single ND is trapped was demonstrated. The stiffness of the trap for quantum dots was twice smaller than the one for gold or silver nanoparticles of similar sizes. The effective radius of quantum dot was 15 nm, the wavelength of the trapping laser was 1064 nm and that leads to the very small contribution of scattering and absorbing force compare to the gradient force. The emission of the quantum dot was 655 nm.

It was reported about two-photon quantum dot excitation during optical trap [15]. The quantum dot was excited while been trapped with the laser used for trapping. Quantum dots with emission wavelength 525, 585, 605, 655, 705 and 800 nm were trapped for this experiment. In the Figure 1.11, the one can see the average value of emission from the trapped quantum dot from the Figure 1.11.

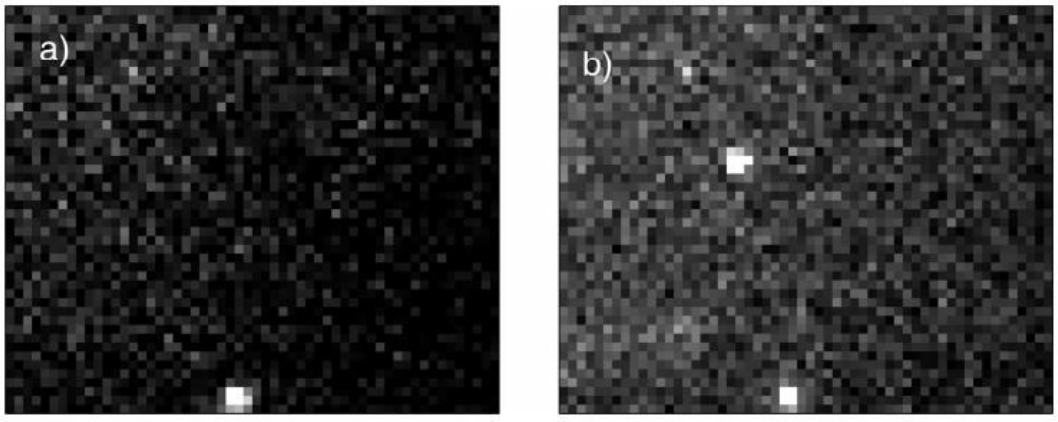

Figure 1.10 Pictures of a biotinylated surface under the optical trap: (a) the surface before a streptavidin-coated quantum dot is trapped (another quantum dot is attached to the surface); (b) the same part of the surface after lowering a trapped streptavidin-coated quantum dot until it attaches to the surface [14].

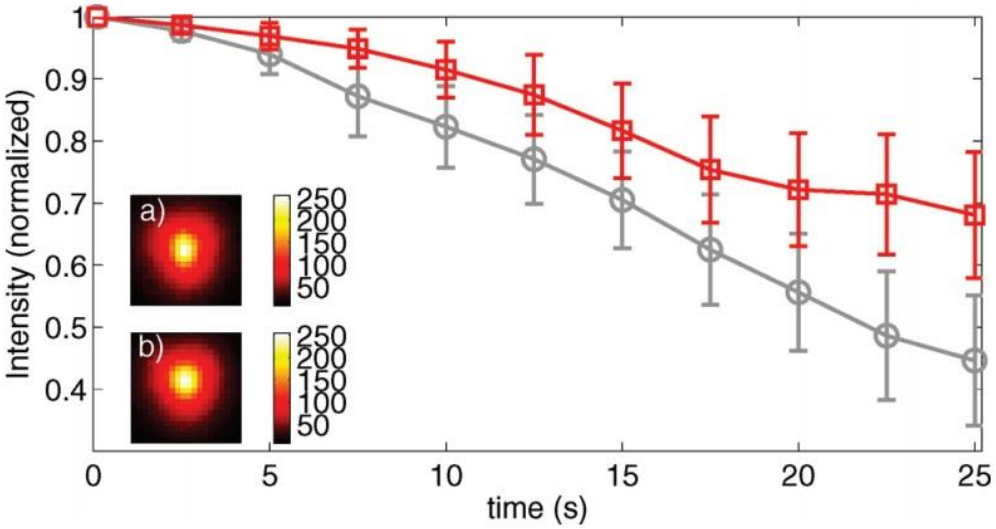

Figure 1.11 Average value of normalized emission from trapped quantum dots aggregates (λ) 605 nm) as a function of time. Upper curve (red squares) shows emission with laser on (Hg lamp off). Lower curve (gray circles) shows emission with both laser and Hg lamp on. Error bars denote SEM. Picture (a) shows emission from a trapped aggregate (no Hg lamp). Picture (b) shows emission from a trapped aggregate with the Hg lamp on [15].

1.4 Research motivation

The objective of our research is to develop a technique based on laser trapping that will provide an ability to apply it for investigations of biological cells. Laser trapping technique has many advantages for biological applications. First of all, it's non-invasive technique with availability to obtain measurements in small volumes with limited access. In addition, it is possible to manipulate the trapped particle in different directions for carrying out the measurements in inhomogeneous media.

First, we develop an approach for measuring viscosity by analyzing the micro displacements of the trapped bead. We trapped 1-μm particles in water–glycerin mixtures and analyzed the dependence of the motion on the viscosity. Based on our calibration with various water–glycerin mixtures, we propose a method for determination of viscosities of unknown liquids with high accuracy.

As a next step, we apply the developed optical tweezers combined with optical microscope for investigations of mechanical properties of the biological cells. By analyzing the cell's structure, we would be able to understand cell processes better, as the intracellular changes corresponds to mechanical changes of the cell.

Investigation of cell parameters will help to detect diseases and provide suitable treatments for cells.

The cell elasticity is one of the important parameter to be studied. We indent the biological cell by trapped polymer fluorescent spheres and study the cell respond. The displacements of the indenter were precisely detected using back focal plane interferometry technique and the visualization of the indentation process is provided by CCD camera.

Chapter 2

Applications of laser trapping

2.1 Optical tweezers for micro bubbles

2.2 Optical tweezers combined with Raman spectroscopy

2.3 Plasmon optical tweezers

2.4 Optical tweezers and STED nanoscopy

2.1. Optical tweezers for trapping micro bubbles

Micro bubbles were consisting of an albumin coating around a gas (octofluoropropane) core [16]. The trapping was possible for bubbles with a diameter as small as 1.5 microns, consisting of albumin shell few tens of nanometers thick. Figure 2.1.1 demonstrates the strongest trapping for bubbles with diameter of trapping circle (1.6-1.8) d_{bubble}. The trapping was impossible for small traps as $d_{trap}/d_{bubble}<1.2$. It was also shown that several micro bubbles can be trapped simultaneously (Figure 2.1.2). The ability to isolate a single micro bubble and to study its dynamics is important for ultrasound imaging and for targeting drug delivery.

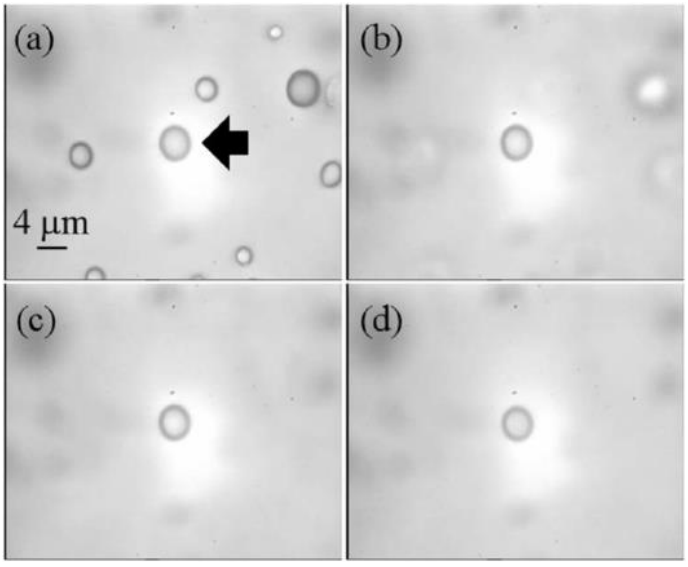

Figure 2.1.1 Trapped bubble. Axial trapping is demonstrated by raising the microscope stage. (a) The bubble (indicated with an arrow) is trapped at the surface of the sample. The microscope stage is raised such that the bubble is moved deeper into the sample. (b) depth of 5-µm, (c) depth of 10-µm, and (d) depth of 50-µm [16].

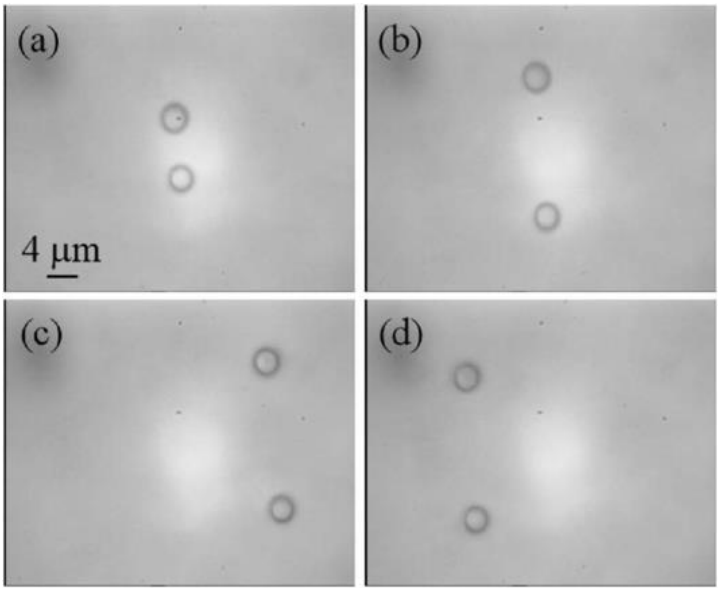

Figure 2.1.2 Two microbubbles trapped in the scanning optical tweezer. (a) Two bubbles, with diameters of 3 and 3.5-µm, are trapped at the surface with separation of 6-µm and moved to a depth of 20-µm below the cover slip. (b) The separation is increased to 16-µm (c) and (d) The trapped bubbles are moved to 10-µm either side of the original trapping position [16].

2.2 Optical tweezers combined with Raman spectroscopy

The combination of laser tweezers and Raman spectroscopy gives a unique technique for optical manipulation and spectroscopic analysis and is applied for individual micro- and nanoscopic objects in physics, chemistry and life sciences [17]. Raman spectroscopy can provide information about species, structures, and molecular confirmation, but has a low sensitivity. The advantage of combination with optical tweezers is that the sensitivity of Raman microspectroscopy can be increased. It was reported about near-infrared Raman spectroscopy of single optically trapped biological cells [18]. The design of the reported system provides high sensitivity and permits real-time spectroscopic measurements of the polymer beads and biological samples. This system is also suitable for the obtaining measurements of single cell, as NIR laser was used for both laser trapping and Raman spectroscopy as well. The absorption coefficient a biological sample for NIR wavelengths is usually lower than for visible ones. Also, the trapping was possible at very low laser powers, like few milliwatts and just for period as short as 2 secs the laser power was increased to few tens of milliwatts to allow sufficient excitation or Raman spectroscopy. First, the system was tested using 2-micron polystyrene latex bead and showed the improvement of Raman shift resolution compare to the previously published spectra. The Raman spectrum of the trapped latex is shown in Figure 2.2.1 Next, the Raman spectrum of trapped single blood cells was obtained and compared with the Raman spectrum of the not trapped cell. From comparison of these spectra one can see that resolution of the spectrum increases dramatically. In Figure 2.2.2 you can see three curves, one for the spectrum of the trapped blood cell, another one for the not trapped cell and last one a subtraction between two mentioned above.

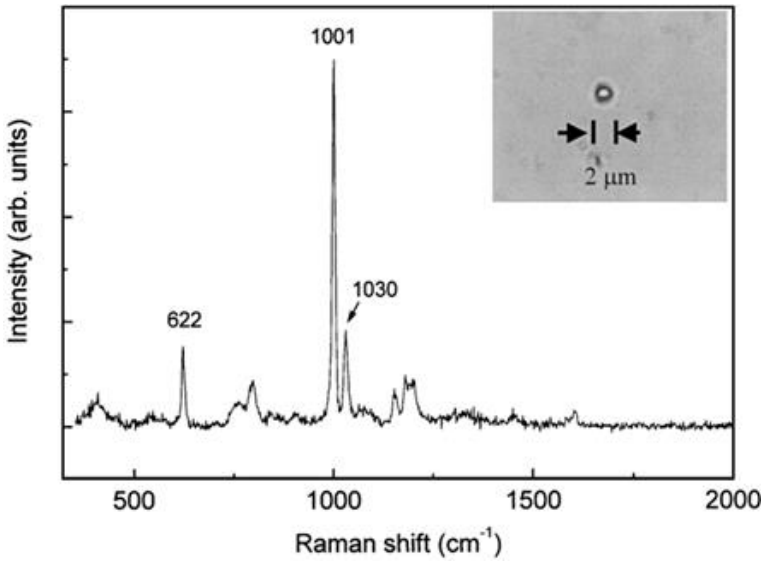

Figure 2.2.1 Raman spectrum and (inset) image of a single polystyrene latex bead of 2.03-mm diameter in an optical trap. The trapping power is 2.0mW and the CCD acquisition time is 2.0 s with 20-mW excitation [18].

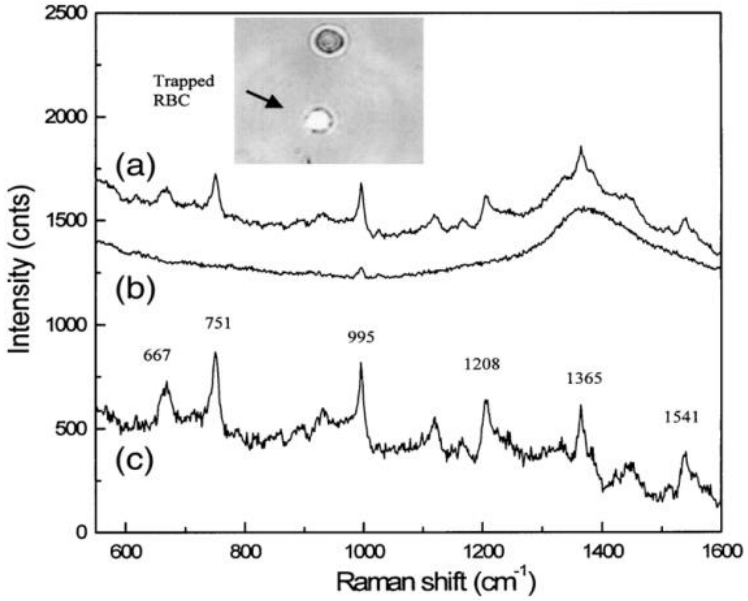

Figure 2.2.2 NIR Raman spectra and image of a single RBC (erythrocyte).Curve (a) is the spectrum recorded when a RBC is trapped, curve (b) is the background without a RBC in the trap, and curve (c) is the subtraction between (a) and (b), magnified by 2 for display [18].

Finally, the spectrum of trapped live and dead yeast cells was obtained (Figure 2.2.3). The significant spectroscopic differences between a living and dead yeast cells were

detectable. The molecular information from single biological cells is useful for diagnosis of cell processes and cellular disorders.

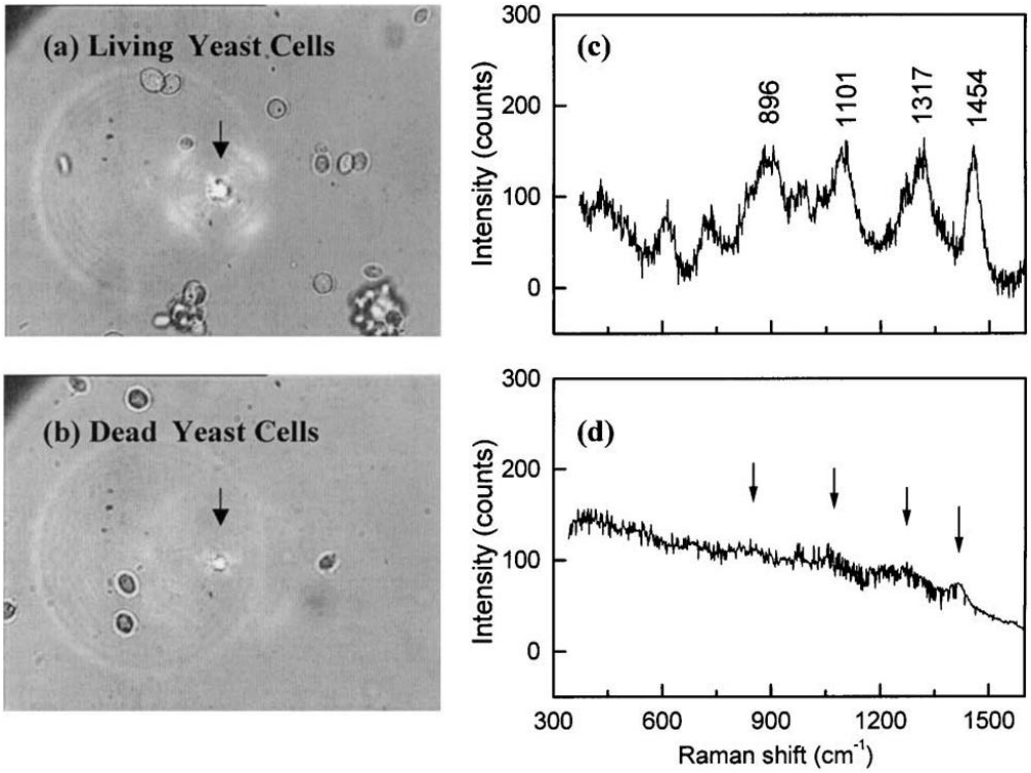

Figure 2.2.3 NIR Raman spectra and images of a single living yeast cell and a dead yeast cell in solution. A significant difference can be seen in the Raman spectra of the living and the dead cells [18].

2.3 Plasmon optical tweezers

The laser trapping force can be enhanced when the optical tweezers interact with tightly localized near field or surface plasmon. The increase in intensity of the focused beam gives an increase of the gradient force, thus resulting in increasing of the trapping force. There are many advantages of plasmon tweezers like harness enhanced optical gradient force, significantly reduced the trapping power, a broad range of attractive applications in biochemistry, sensing, and on-chip microfluidic cell sorting. However, there are disadvantages as plasmon tweezers requires high-precision fabrication techniques which are time-consuming, expensive and produce

low yield of product. Also, specific optical geometry alignment (Kretschmann configuration) with the specific incident angle for activating the trapping mode has a narrow window what limits the applications of the proposed plasmon tweezers. Figure 2.3.1 shows the trapping is realized for the proposed plasmonic random systems with the stochastic localized field of surface plasmons [19].

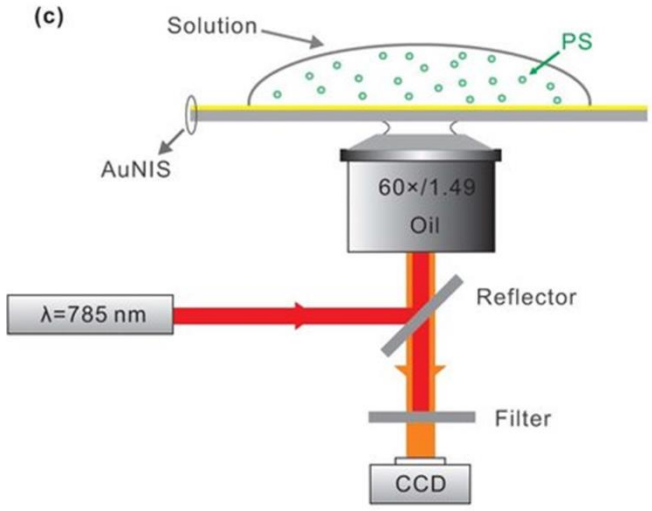

Figure 2.3.1. Schematic of optical setup for the optical tweezers using plasmonic random systems [19].

Random structures sample in the form of gold nano-island substrate (AuNIS) were easily prepared by using metal deposition followed by thermal annealing and are shown in Figure 2.3.2 [19].

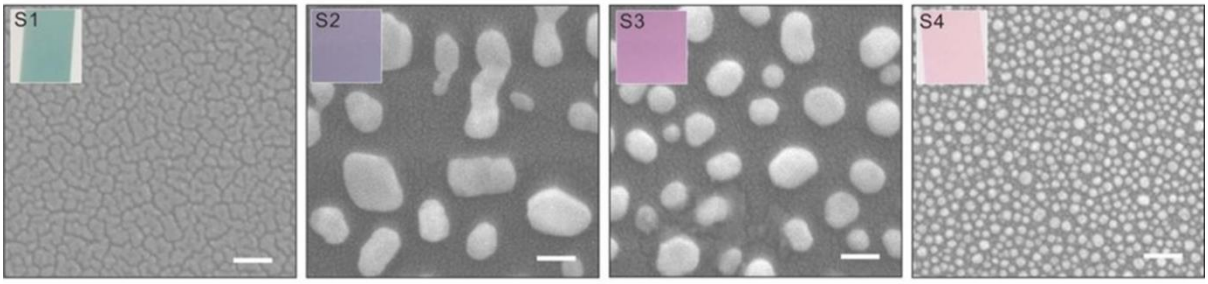

Figure 2.3.2. Plasmon random systems. For S1 the nanogaps were 10 nm, for S2 the gold nano islands were 80-300 nm, for the S3 30-140nm and for the S5 15-35 nm respectively. Scale bar is 100 nm [19].

Finally, it was shown that trapping and manipulating of polystyrene spheres are achievable with very low power density which isn't enough for trapping without random plasmonic structures. Also, the trapping of polystyrene spheres doesn't require high numerical aperture lenses as it does normally. It was shown, that within the trapping process, the beads not only form a two-dimensional compact assembly, but they also stack vertically layer by layer into a three-dimensional tower cluster.

Plasmonic tweezers have been successfully applied for trapping and organizing Escherichia coli cells. One of possible applications is the immobilization of a target microorganism and moving it to any specific position without damaging biological cells.

2.4 Optical tweezers and STED nanoscopy

The optical tweezers are widely used technique combination with which gives an improvement of many other ordinary available techniques. With optical tweezers, other techniques are able to get unique results as in case of combination of STED nanoscopy with optical tweezers for revealing protein dynamics on densely covered DNA [20]. The designed instrument combines optical tweezers with beam scanning confocal fluorescence microscopy and STED nanoscopy. The beam scanning confocal fluorescent microscopy and STED nanoscopy provides the imaging of protein dynamics on DNA and distinguishing individual labeled proteins and protein filaments at high protein density. The optical tweezers play important role in the increasing the resolution of imaging of resolving protein dynamics. This is achieved due to stretching the DNA by two trapped polymer spheres attached to the both sides of the DNA as shown in Figure 2.4.1 (a). This results in the decreasing of the motion of DNA and enabling the resolving of dynamic of proteins. An excitation that is scanned over DNA is marked by green, for optical trapping two traps were created and controlled independently by tip-tilt mirrors M_1 and M_2, as demonstrated in Figure 2.4.1 (b). The displacements of trapped polymer spheres were detected by position sensitive detectors using back focal interferometry. The observation of manipulation of trapped microspheres is provided by CMOS camera. The violet laser supplies

STED and other three beams (640 nm, 543 nm and 467 nm) filtered from a supercontinuum spectrum using an acousto-optical tunable filter (AOTF) for exciting the fluorescence.

Precise control of tension of DNA allows achieving high-resolution imaging. If the tension to DNA is applied, thermal fluctuations of suspended DNA will not blur the images of DNA-bound proteins. The optical tweezers can provide the needful tension of DNA, resulting in decreasing fluctuations of DNA. Figure 2.4.2 proves the advantages of this technique. The confocal microscopy can't resolve individual protein trajectories at high densities, as shown in Figure 2.4.2 (a). However, using STED combined with optical tweezers allows observation of individual proteins trajectories along the DNA at a subdiffraction resolution, which is enhanced by 6 times over confocal imaging.

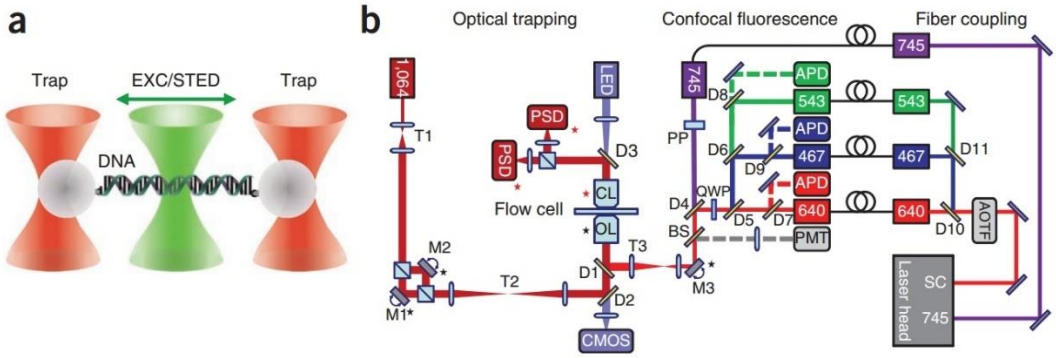

Figure 2.4.1 TFAM binding and diffusion dynamics on optically stretched DNA [20].

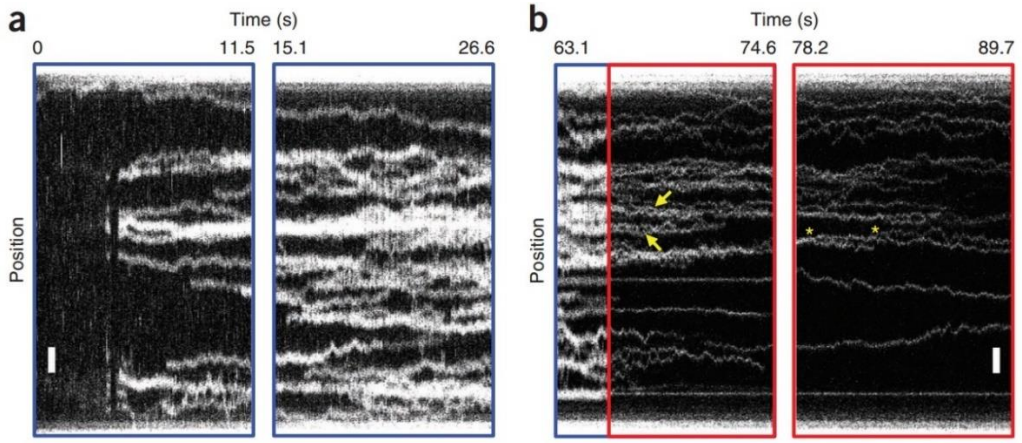

Figure 2.4.2 TFAM binding and diffusion dynamics on optically stretched DNA [20].

Chapter 3

The theory of laser trapping

3.1. The optical forces

The optical forces that arise in laser trapping can be explained in terms of transfer of momentum from the trapping beam to the particle. The change of momentum occurs due to that incident beam is reflected and refracted while being focused on the particle to be trapped. The trapping force can be explained as a sum of two forces, gradient and scattering force as shown in the Figure 3.1.

Next, we will discuss about the nature of this forces and then about regimes of trapping.

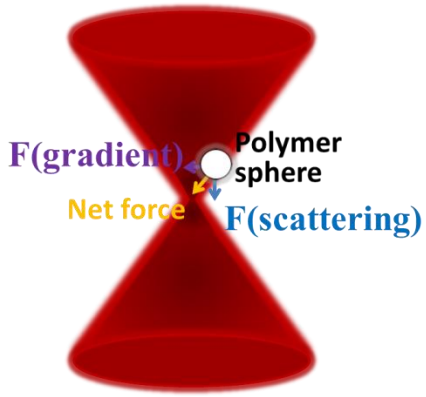

Figure 3.1. The optical forces in the trap.

3.1.1 Gradient force:

The atoms or ions are polarized and when the laser beam is irradiated to the particle it creates a dielectric response. If the laser beam is monochromatic, linearly polarized, the induced dipole moment is:

$$\vec{p} = \alpha\vec{E} \qquad (3.1.1.1)$$

where α is a complex polarizability of the particle of the particle to the surrounding medium and can be written as follows:

$$\alpha = \alpha' + i * \alpha'' = n_m^2\tau^3\left(\frac{n_c^2-1}{n_c^2+2}\right) \qquad (3.1.1.2)$$

An electrostatic potential will be created as follows:

$$U = -\vec{p} * \vec{E} \qquad (3.1.1.3)$$

In the light field with the spatially varying intensity the gradient will occur and the gradient force can be written as:

$$\vec{F}_{grad} = -\nabla U = -p\nabla\vec{E} = -\alpha(E\nabla)\vec{E} \qquad (3.1.1.4)$$

After (2) is inputted into (4):

$$\vec{F}_{grad} = \frac{n_m^3 r_p^3}{2}\left(\frac{n_c^2-1}{n_c^2+2}\right)\nabla\vec{E}^2 \qquad (3.1.1.5)$$

The gradient force is linearly dependent on the spatial variation of the intensity of the light field and on the dielectric contrast of the particle relative to the surrounding media. This phenomenon can be described by the Clausius-Mossotti relation, according to which for particles with a refractive index higher than the surrounding medium, the gradient force acts toward the point of highest intensity and

for particles with a lower refractive index acts toward the point of minimum light intensity.
The trapping force can be characterized as a Hookean spring with stiffness k:

$$\vec{F} = -k\vec{r} \tag{3.1.1.6}$$

where r-radius of the optical trap

The laser trap will be characterized as an almost harmonic potential if it's created by focused Gaussian beam. The micrometer particle in the viscous fluid shows an exponential dumped motion:

$$x(t) = x_o \exp\left(\frac{k}{6\pi\eta\tau}t\right) \tag{3.1.1.7}$$

$$\tau = \frac{6\pi\eta r_p}{k}$$

where t is correlation time, η is the viscosity of the surrounding medium, k is the trap stiffness and r_p is friction constant (Stoke's law).

3.1.2 Scattering force

The scattering force occurs because of scattering light on the particle to be trapped because of photons having momentum. This force is pointed in the direction of propagation of laser beam and is dependent on the beam intensity. A single photon with energy E has a momentum:

$$\vec{p} = \hbar\vec{k} = \frac{\vec{E}n_m}{c} \tag{3.1.2.1}$$

The momentum change means the force change and the scattering force can be calculated as

$$\overrightarrow{F_{scat}} = \frac{n_m\sigma\langle S\rangle}{c} \tag{3.1.2.2}$$

where $n_m$is the refractive index of the surrounding medium, $\langle S \rangle$ is the time-averaged Poynting vector, *c* is the speed of light, and σ is the particle's optical cross section. The Rayleigh scattering cross-section for the spherical dielectric particle is:

$$\sigma = \frac{8}{3}\,\pi \left(\frac{2\pi n_m}{\lambda}\right)^4 r_p^6 \left(\frac{n_c^2-1}{n_c^2+2}\right)^2 \qquad (3.1.2.3)$$

Where $r_p$is the particle radius, $n_c = \frac{n_p}{n_m}$is the refractive index contrast between the particle (n_p) and the medium (n_m), $\frac{2\pi}{\lambda}$ is a wave vector of the trapping light. Then the scattering force:

$$F_{scat} = \frac{128\pi^5 r_p^6}{3\lambda^4}\left(\frac{n_c^2-1}{n_c^2+2}\right)\frac{n_m}{c} I_0 \qquad (3.1.2.4)$$

From Eq. (11) one can see that the scattering force is dependent on the light intensity, the wavelength of the trapping light, the particle size, and its refractive index contrast against the medium to be immersed in.

3.2 Regimes of the trapping

Depending on the ratio of the trapping wavelength to the radius of the particle to be trapped, the trapping forces can be explained in the regime of ray optics or electromagnetic interactions. When the trapped sphere is much larger than the wavelength of the trapping laser the conditions for Mie scattering are satisfied and optical forces can be computed from simple ray optics. On the other hand, when the trapped sphere is much smaller than the wavelength of the trapping laser, the conditions for Raleigh scattering are satisfied and optical forces can be calculated by treating the particle as a point dipole [21].

3.2.1 Ray optics regime

In the ray optics regime, the laser beam is treated as a decomposition of rays which refract and bend due to the trapping particle to be placed in the light path. To create a trap, a continuous, diffraction limited monochromatic beam should be focused by a high numerical aperture lens. The Figure 3.2.1.1 illustrates the few examples of how trapping occurs in the ray optics regime. The red region represents the gradient of intensity of the laser beam with the maximum in the center, in the brightest region which corresponds to the focus region. The blue sphere is a particle to be trapped; the gray rays represent the rays, the thickness of which corresponds to the intensity of rays. Because the rays have the same intensity in the case of (a), the particle will not be pushed left or right. Still rays are slightly bent inwards, creating a force that pulls the bead towards the laser source. In case of (b) the particle is displaced slightly to the right of the focus of laser beam, resulting in different intensity rays to be bent and in the net force pointed to the left.

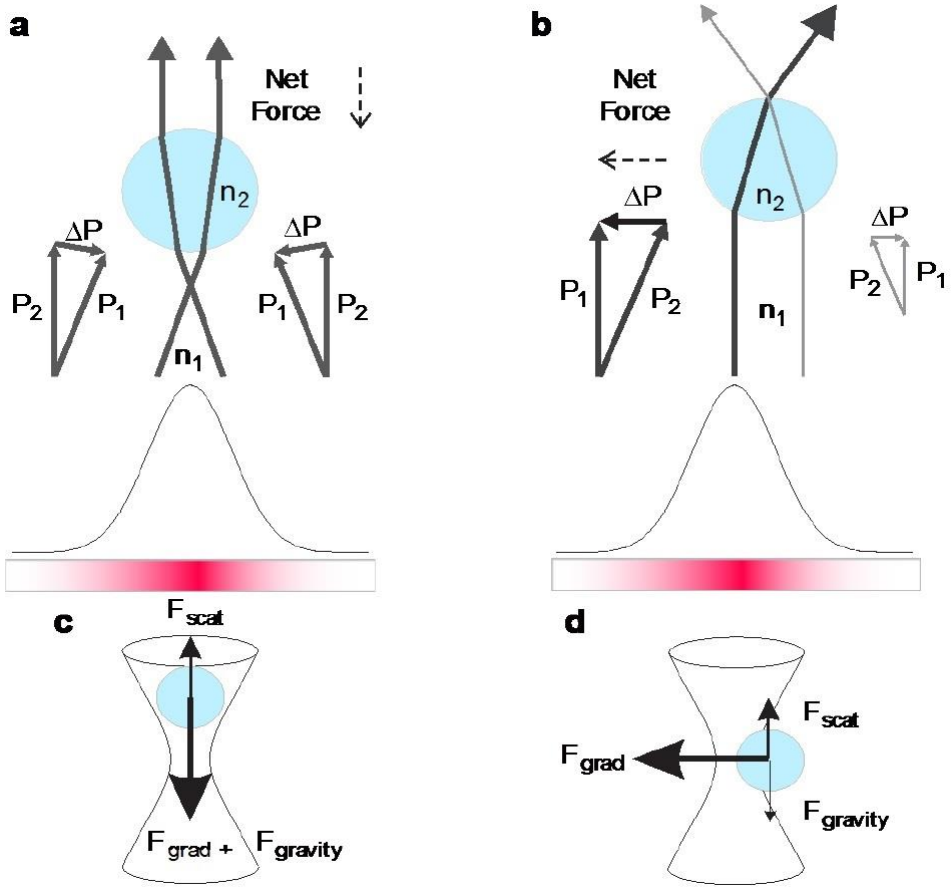

Figure 3.2.1.1 Schematic of the optical forces in the ray-optics regime. Summing the rays gives an (a) axial force due to vertical displacement from trap center; (b) radial force due to lateral displacement from trap center. Considering gravity and scattering, (c) the axial and (d) radial gradient force must be the dominant component to form an optical trap [22].

There is another approach to explain the trapping in ray regime. We can think of trapped particles as a weak positive lens as shown in Figure 3.2.1.2. If the lens is at the focus of the beam, the rays pass through the center of the lens and are undeviated—the optical force is zero. If the lens is before the focus, it increases the convergence of the beam, and therefore decreases the momentum flux. The lens gains the momentum the beam loses, and there is a force in the direction of propagation. If the lens is after the focus, it decreases the divergence of the beam, and hence increases the momentum flux, resulting in a restoring force toward the focus. If the lens is displaced sideways, the beam is deflected toward the centerline of the lens, gaining lateral momentum. The lateral reaction force on the lens acts toward the beam axis [21].

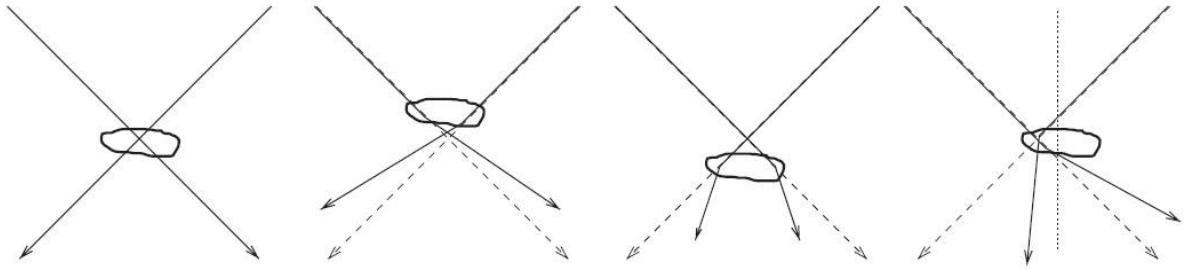

Figure 3.2.1.2 The force exerted on a particle in optical tweezers can be understood in terms of changes in the momentum flux of the trapping beam. For axial forces, the important principle is that the more convergent or divergent the beam is, the lower the axial momentum flux. For radial forces, the direction of the beam is the key principle. The trapped particle can be thought of as a weak positive (converging) lens [21].

For quantitate analysis we will refer to the explanations by Arthur Ashkin [23]. In Figure 3.2.1.3, there is a model proposed by Wright [24], the focal point is f, along the Z axis of the sphere. The convergence angle corresponds to ϕ for X axis, β for Y axis and total force consists of sum of contributions of all beam rays and r is the radius of aperture. The beam radius is marked by ω.

The main fail of this model is that it tries to describe the single beam gradient in terms of both wave and ray optics. Using TEM_{OO} Gaussian mode beam propagation formula, they describe the focused trapping beam and stay that the ray directions of the individual rays are perpendicular to the Gaussian beam phase fronts. Since the curvature of the phase fronts vary considerably along the beam, the ray directions also change, from values as high as 30° or more with respect to the beam axis in the far-field, to 0° at the beam focus which is physically incorrect [24]. They also calculate for beams with relatively small convergence angle what is not common for beams focused with required high numerical aperture objective.

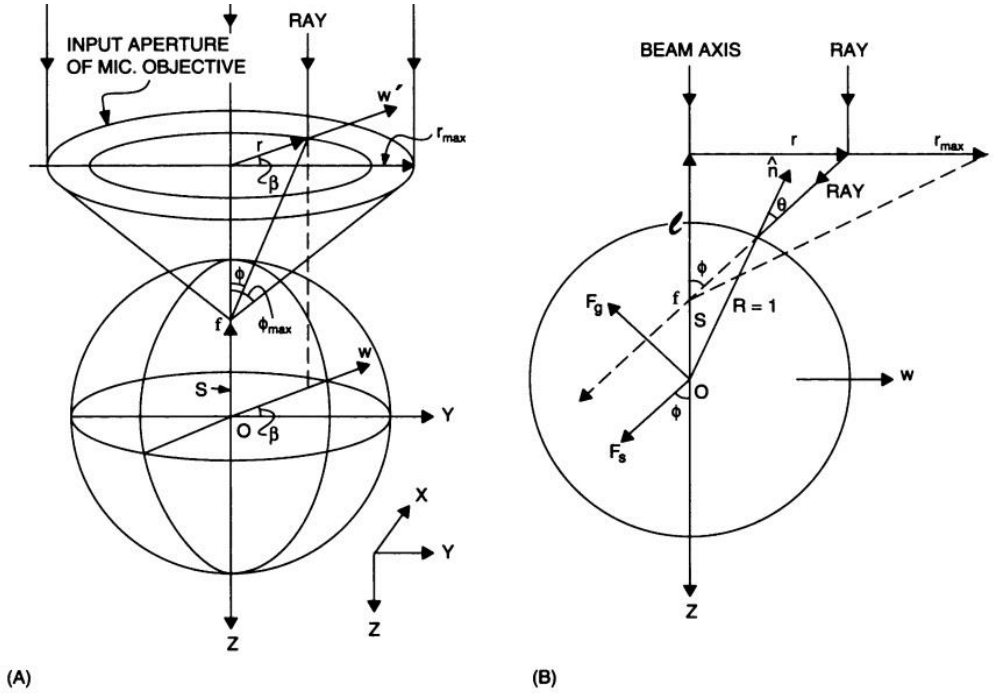

Figure 3.2.1.3 (A) Single beam gradient force trap in the ray optics model with beam focusflocated along the Z axis of the sphere. (B) Geometry of an incident ray giving rise to gradient and scattering force contributions F_g and F_s. O – the center of the sphere, S – possible position of focus of the trapping beam [23].

The dielectric sphere is heated by a single ray of power P at an angle of the incidence θ as shown in Figure 3.2.1.4. The total force will be a sum of contributions due to the reflected ray of power PR and the infinite number of emergent refracted rays of successively decreasing power PT^2, PT^2R,….PT^2R^n, …[23]. R and T are the Fresnel reflection and transmission coefficients of the surface at θ. The net force consists of two components F_z and F_y:

$$F_z = F_s = \frac{n_1 P}{c}\left\{1 + Rcos2\theta - \frac{T^2[\cos(2\theta-2r)+R\cos 2\theta]}{1+R^2+2R\cos 2r}\right\} \qquad (3.2.1.1)$$

$$F_y = F_g = \frac{n_1 P}{c}\left\{R\sin 2\theta - \frac{T^2[\cos(2\theta-2r)+R\cos 2\theta]}{1+R^2+2R\cos 2r}\right\} \qquad (3.2.1.2)$$

F_s is a scattering force pointing the particle in the direction of incident ray, F_g is a gradient force pointing in the direction perpendicular to the ray.

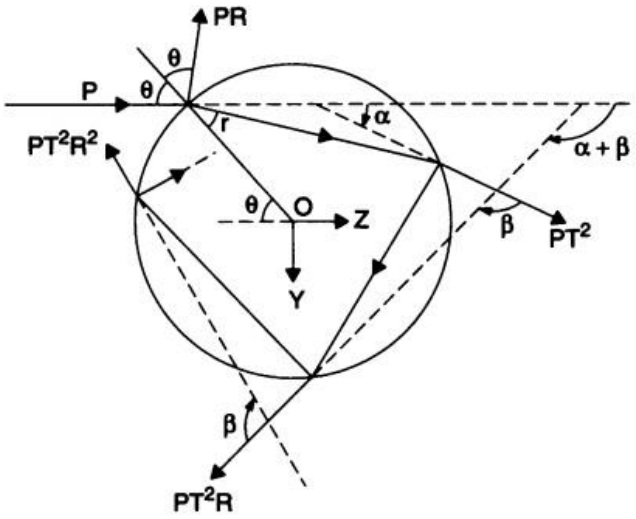

Figure 3.2.1.4 Geometry for calculating the force due to the scattering of a single incident ray of power P by a dielectric sphere, showing the reflected ray PR and infinite set of refracted rays PT^2R''[23].

3.3.2 Rayleigh regime

In case when the radius of the trapped particle is much smaller than the light wavelength, the particle is considered like induce dipole in the electromagnetic field (Figure 3.3.2.1). A plane wave of intensity I_0 striking a Rayleigh particle scatters light moment in a symmetrical dipole radiation pattern giving rise to a net force in the direction of the incident light, which is called the scattering force [25]:

$$F_{scat} = \frac{P_{scat}}{c} = \frac{I_o}{c}\frac{128\,\pi}{3}\frac{r^6}{\lambda^4}\left(\frac{m^2-1}{m^2+2}\right)^2 n_b \qquad (3.3.2.1)$$

where m is the effective index of refraction and is equal to the ratio of the index of refraction of the particle n_a to that of the medium n_b.

Then, if the particle is displaced in the beam where there is a gradient of intensity, the additional gradient force will pull the particle into the region of the highest intensity. The gradient force on Rayleigh particles can be understood most simply in terms of the force optical field gradient on the optically induced dipole moment of the particle [25]:

$$F_{grad} = -(1/2)\,\alpha\,\nabla E^2 \qquad (3.3.2.2)$$

Where α is a polarizability of the particle and determined as follows:

$$\alpha = r^3 \left[\frac{m^2-1}{m^2+2}\right] n_b^2 \qquad (3.3.2.3)$$

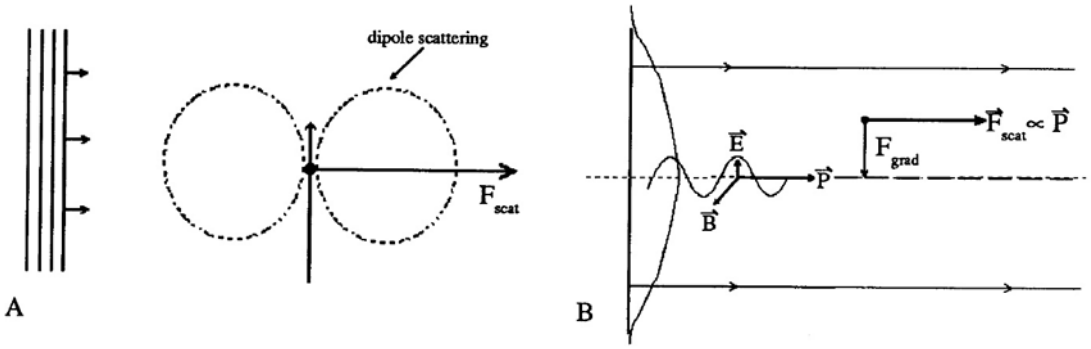

Figure 3.3.2.1 (A) The force exerted by a beam of photons on a Rayleigh particle (size less than wavelength) is due to the interaction of electric vector E of the light with the electric dipole of the particle. (B) The gradient force on Rayleigh particles in a beam that is more intense at the centerline. The scattering force propels particles in the direction of the Pointing vector (direction of the beam) as in (A), while the intensity gradient $\boldsymbol{\nabla E^2}$ draws particles toward the beam axis by a force directly proportional to the polarizability of the particle α and the gradient of the square of the electric vector [25].

Thus, the gradient force points in the direction of the intensity gradient and pulls high index of refraction Rayleigh particles into the high intensity region of the beam.

Chapter 4

Experimental optical setup for laser trapping

4.1. Designed experimental setup for laser trapping

4.2. The required minimum laser power for stable trapping.

4.3. The steering of the trapped polymer sphere.

4.1. Designed experimental setup for laser trapping

We have developed the optical setup, which combines laser trapping technique with optical tweezers demonstrated at the Figure 4.1.1. For laser trapping near infrared laser was applied. The emission wavelength of Nd: YVO_4 is 1064 nm. The pulse width at 20 kHz is 10 nanoseconds and the maximum laser power is 10W. The near-infrared laser has an advantage for laser trapping as many biological objects have an absorption window at this range.

From this Figure one can the backside of the microscope and where the trapping laser enters the microscope. The laser beam after refracted by the mirrors and passed through the beam expander is irradiated to the galvano mirror. The galvano mirror plays an important role in steering the laser beam. The mirror was purchased from Throlabs and has dual axis systems comprise two mirrors and motor assemblies, an X_Y mounting bracket, two driver cards and mountings with heat sink. The galvano mirror (Figure 4.1.2) with protected silver mirrors was chosen in order to meet our goals. Mirror is moved by the motor and capacitive position detector feeds back mirror position to the system. The galvano mirror motor features a moving

magnet, which means that the magnet is part of the rotor and the coil is part of the stator, this configuration provides faster response and higher system-resonant frequencies when compared to moving coil configurations [26].

After laser beam is refracted by galvano mirror and height changed by mirrors, it enters the microscope. The microscope can work as light transmitted or fluorescent one.

In the Figure 4.1.3, the schematic of microscope is demonstrated. The laser beam is focused by high numerical aperture lens which is placed in the objective turret, under the sample stage. Position sensitive detector was used for detection of the position of the trapped particle. Before the light reached the detector, it was focused and magnified by condenser lens, then filtered out by filters placed in the filter turret. At the same turret, in order to reflect the light coming from halogen lamp, the mirror was placed. The observation of the trapped particle was provided by CCD camera.

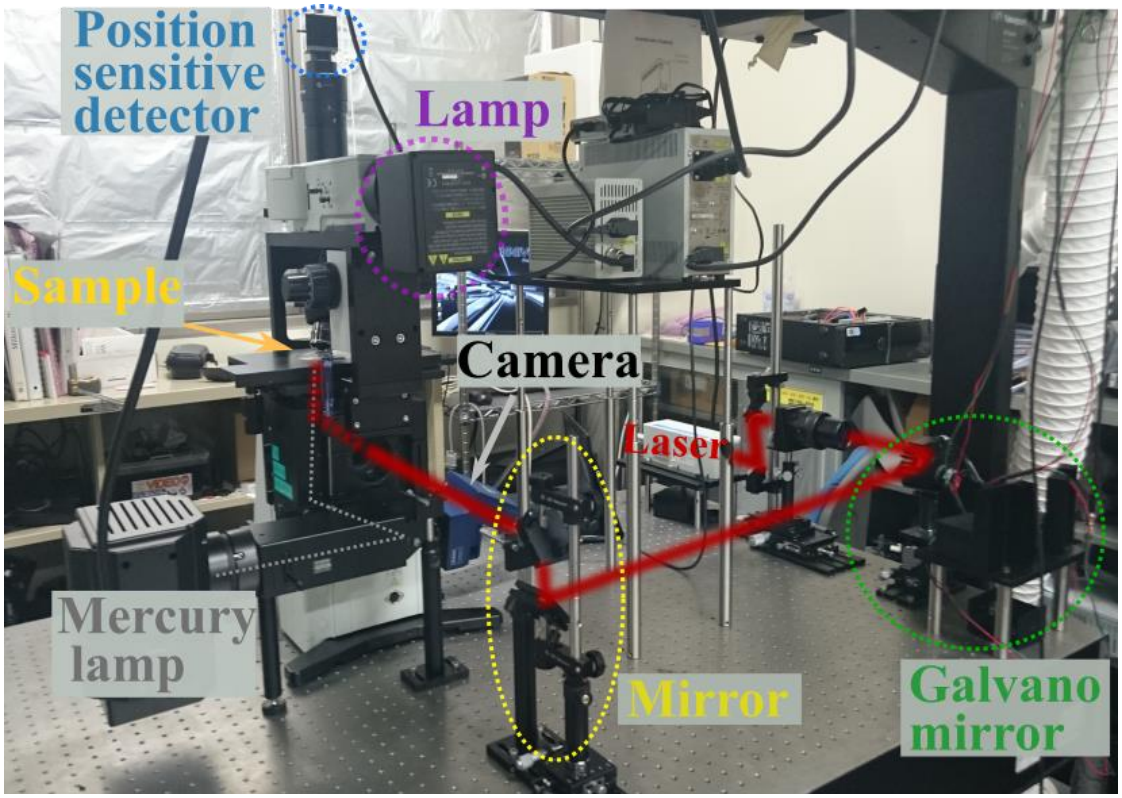

Figure 4.1.1 The optical setup of laser tweezers combined with optical microscope. The trapping laser is marked by red.

Figure 4.1.2 The demonstration of the laser steering by galvano mirror. The laser beam is marked by red line. White arrows demonstrate the directions of the mirror motor movement. The arrows demonstrate the possible steering directions

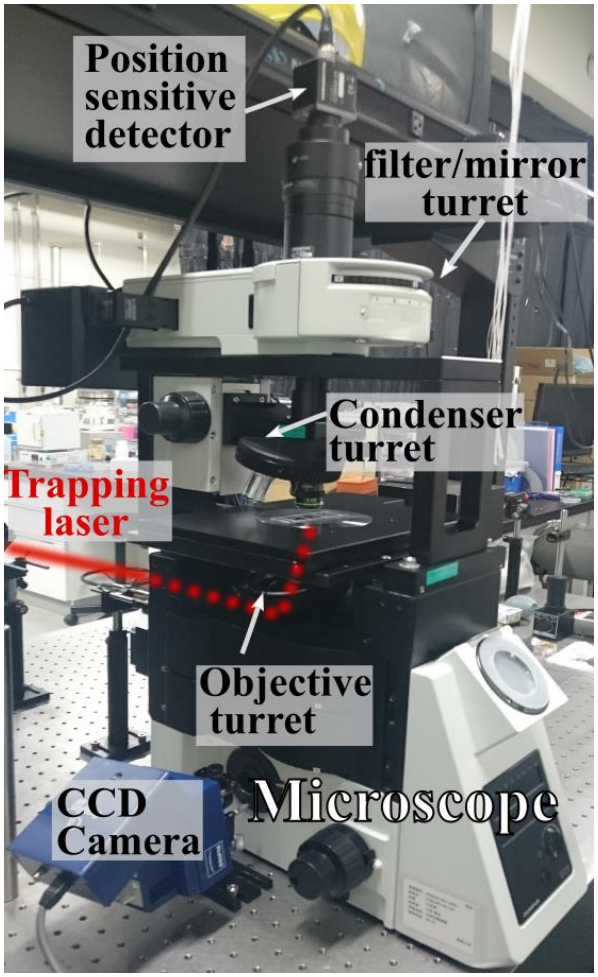

Figure 4.1.3 The demonstration of the optical microscope used for laser trapping.

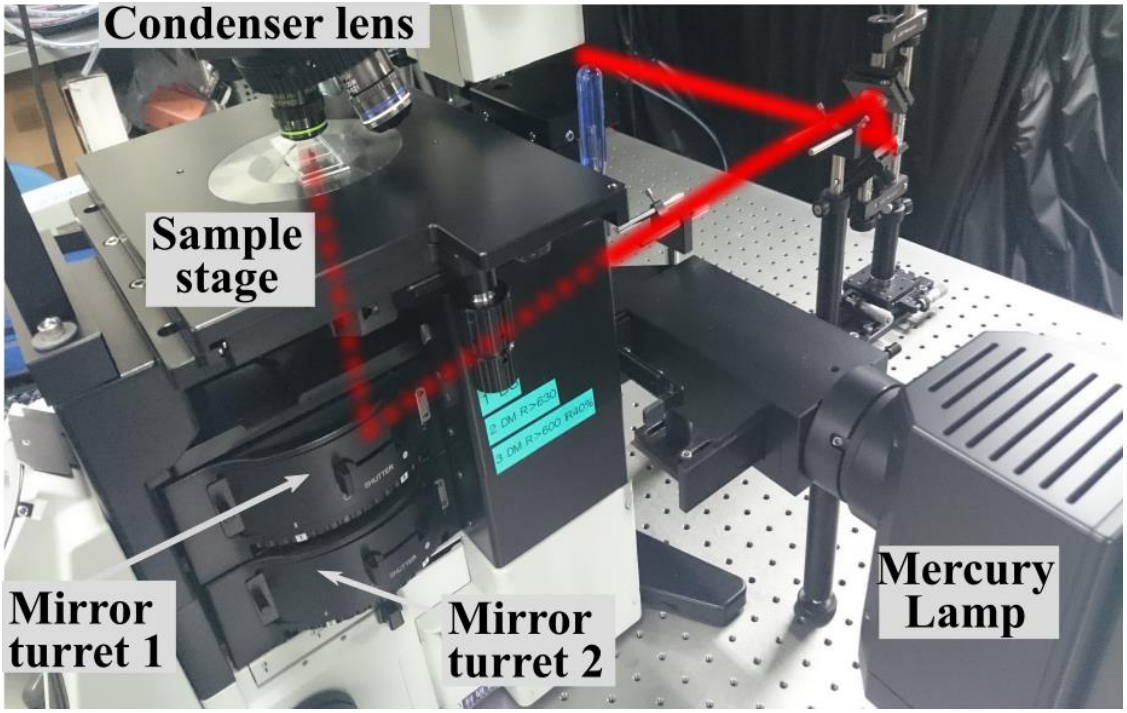

Figure 4.1.4 The demonstration of the modified microscope turrets and the propagation of the trapping laser.

In order to combine the microscope with optical tweezers, the extra mirror turret was placed as one can see in the Figure 4.1.4. In order to refract the trapping laser in the direction of the objective lens and to allow the halogen lamp light to be transmitted the dichroic mirror was placed to the turret 1. The light from mercury lamp is irradiated to the mirror turret 2. The turret 2 has 3 specific filters for the fluorescence excitation with B-, G- and U-excitation as shown in Figure 4.1.5. The green, red, ultra violet excitation wavelengths are available for the exciting different fluorescent objects. The objective lens is placed under the sample table.

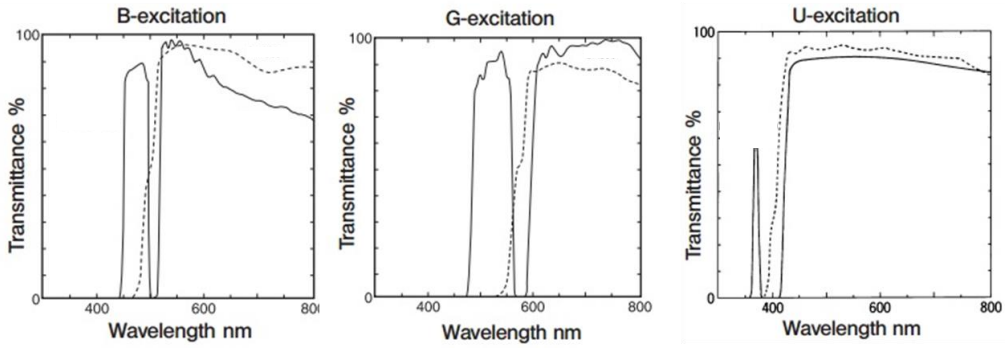

Figure 4.1.5 Spectral characteristic of filters from mirror turret 2 [27].

4.2. The required minimum laser power for stable trapping

In this chapter, we will discuss about minimum laser power needed for trapping and about conditions of stable trapping. Also, we will demonstrate the examples of stable and not stable trapping.

First, 1 micron polymer spheres were immersed in water. Then the single particle was trapped and manipulated by galvano mirror scanning system with frequency 1Hz. At the Figure 4.2.1 the one can see the displacement of the trapped polymer sphere with the time. The motion of trapped particle was quite stable.

Next, in order to find the smallest required laser power for trapping, the laser power was gradually decreased. At the moment of laser power as small as almost 2mW, the laser trapping was still possible; however, the manipulation of the trapped particle wasn't stable, as shown in Figure 4.2.2.

The one can see the clear difference of the displacements of 1 micron polymer sphere between Figure 4.2.1 and Figure 4.2.2. Those results in understanding, that even though the trapping is possible at low laser powers, it doesn't mean that the trapping force will be enough strong that the trapped particle can follow the laser beam.

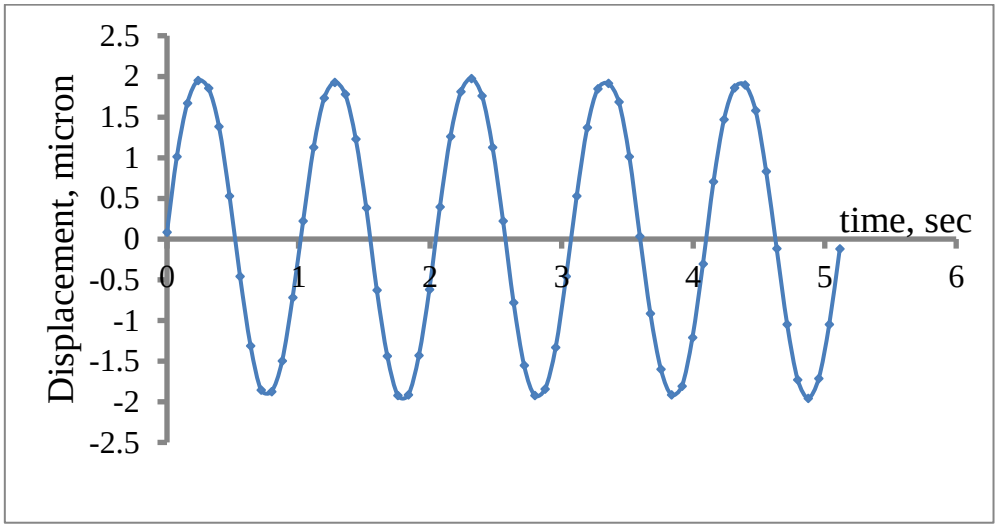

Figure 4.2.1 The demonstration of the manipulation of the trapped polymer sphere. The 1 micron polymer sphere was trapped in water with frequency 1Hz and amplitude of 4 microns.

For further manipulations, we should consider not about the minimum laser power for trapping, but the minimum laser power for the required manipulation.

The same experiment was provided for the 5-micron polymer spheres at the same laser powers as for 1 micron particles. Figure 4.2.3 demonstrates the stable trapping for this case of 5-micron. In Figure 4.2.4, the one can see that the manipulation of the trapped sphere is unstable. From this result, we also can see that the trapping force for the 5 micron particles is weaker than for the 1 micron particles.

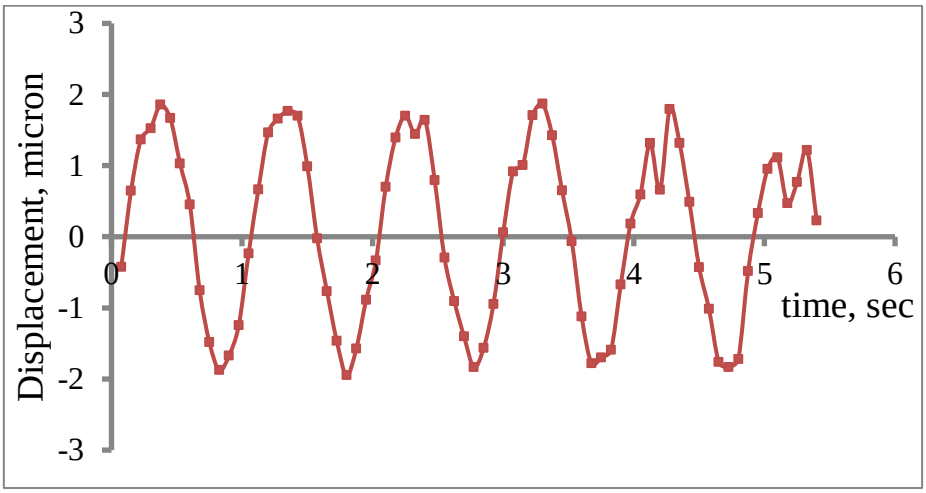

Figure 4.2.2. The demonstration of the manipulation of the trapped polymer sphere with laser power not enough strong for manipulations of trapped particles.

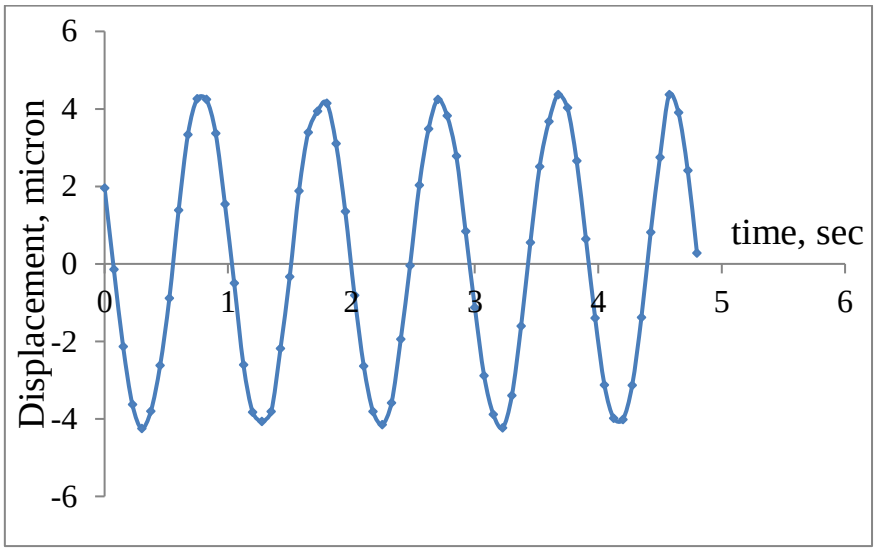

Figure 4.2.3 The demonstration of the stable manipulation of the trapped polymer sphere. The 5-micron polymer sphere was trapped in water with frequency 1Hz.

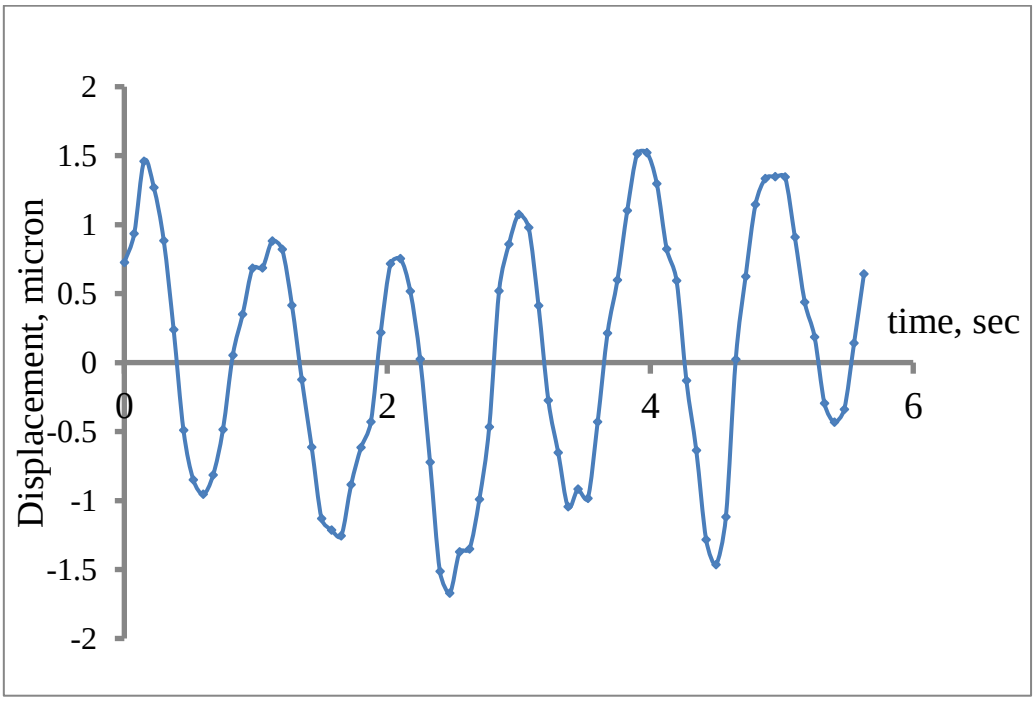

Figure 4.2.4 The demonstration of the unstable manipulation of the trapped polymer sphere. The 1 micron polymer sphere was trapped in water with frequency 1Hz and amplitude 4-micron.

The displacements of trapped particles were detected using CCD camera and analyzed by Video tracking software. At the figure 5, we demonstrate the example of manipulation of the 5-micron polymer sphere.

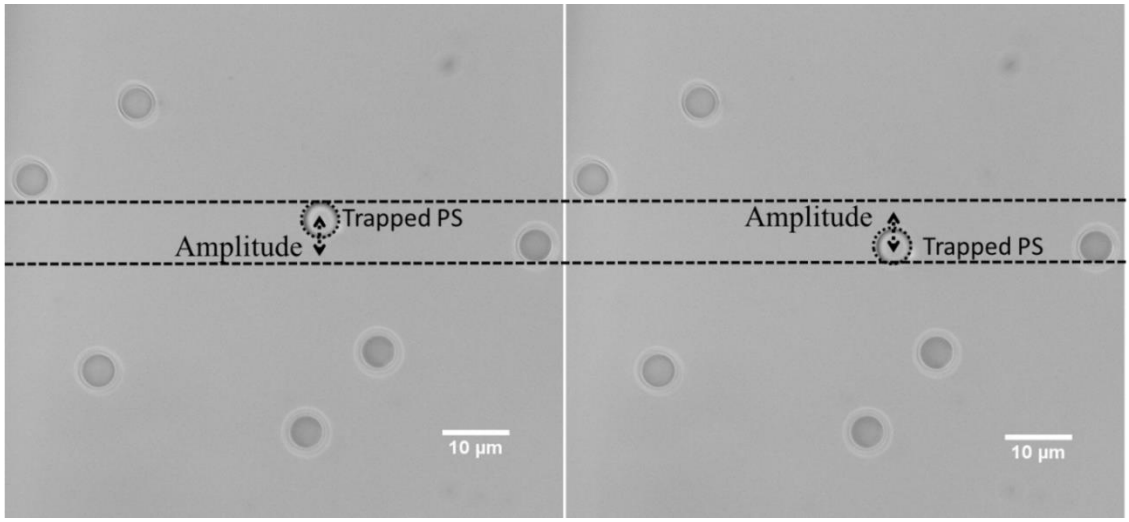

The demonstration of manipulation of 5-micron polymer sphere (PS). The images were obtained using CCD camera. The trapped polymer sphere and the maximum displacements are marked by black dash lines.

4.3. The steering of the trapped polymer sphere

The polymer sphere is steered by Galvano mirror system. The frequency and the trajectory can be controlled. In this section, we want to demonstrate the possible manipulation of the trapped polymer sphere.

The 3-micron polymer spheres were immersed in water with low density and after the sphere riches the area of laser beam, it was pulled to the focal region, what means it was trapped. Next, we demonstrate the series of pictures, which show the possible trajectory of the manipulation of the trapped polymer sphere. The trapped particle is manipulated following elliptical trajectory.

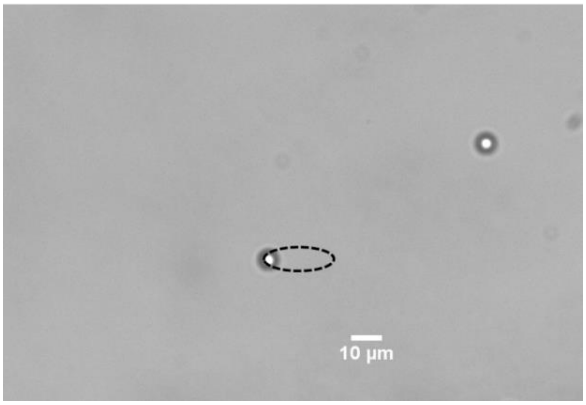

Figure 4.3.1 Demonstration of the possible manipulation of the trapped particle. The trajectory of manipulation of the trapped particle is marked by black dashed line. The size of the polymer sphere was 3-micron. The trapped particle moves clockwise. (a) The trapped particle is at the starting point.

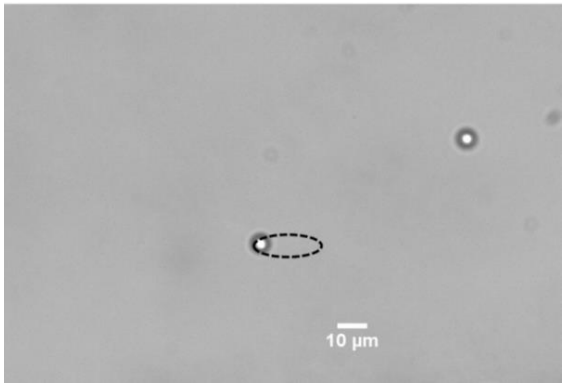

Figure 4.3.2 Demonstration of the possible manipulation of the trapped particle. The trajectory of manipulation of the trapped particle is marked by black dashed line. The size of the polymer sphere was 3-micron. The trapped particle moves clockwise. (b) The trapped particle started motion, slightly above the starting point.

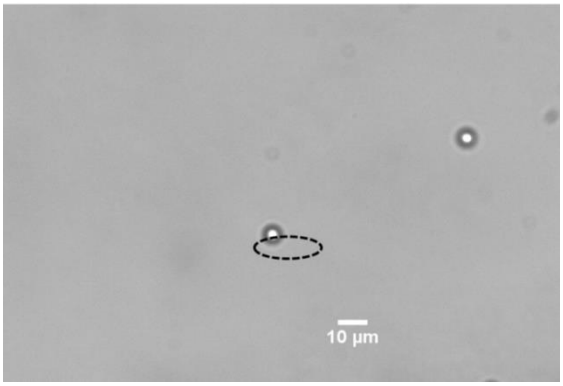

Figure 4.3.3 Demonstration of the possible manipulation of the trapped particle. The trajectory of manipulation of the trapped particle is marked by black dashed line. The size of the polymer sphere was 3-micron. The trapped particle moves clockwise from the starting point.

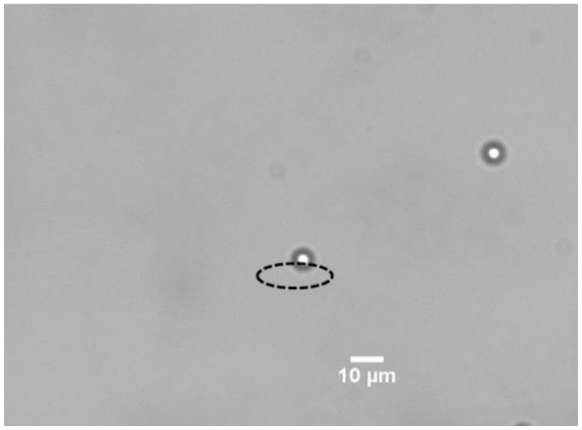

Figure 4.3.4 Demonstration of the possible manipulation of the trapped particle. The trajectory of manipulation of the trapped particle is marked by black dashed line. The size of the polymer sphere was 3-micron. The trapped particle moves clockwise.

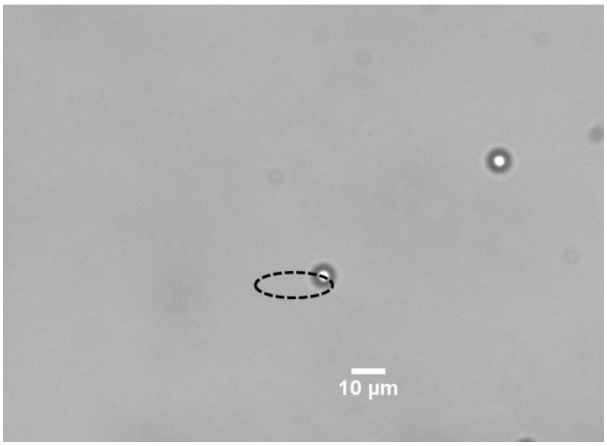

Figure 4.3.5 Demonstration of the possible manipulation of the trapped particle. The trajectory of manipulation of the trapped particle is marked by black dashed line. The size of the polymer sphere was 3-micron. The trapped particle moves clockwise.

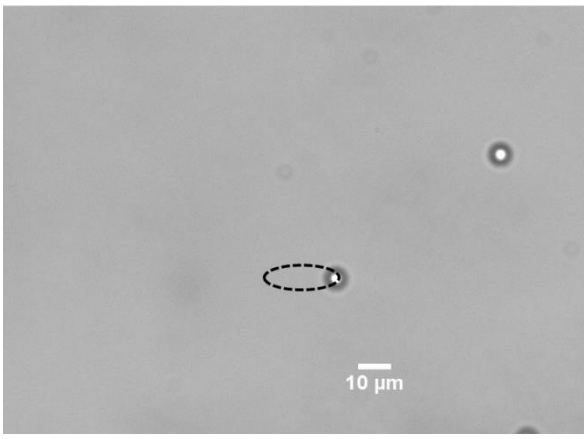

Figure 4.3.6 Demonstration of the possible manipulation of the trapped particle. The trajectory of manipulation of the trapped particle is marked by black dashed line. The size of the polymer sphere was 3-micron. The trapped particle moves clockwise.

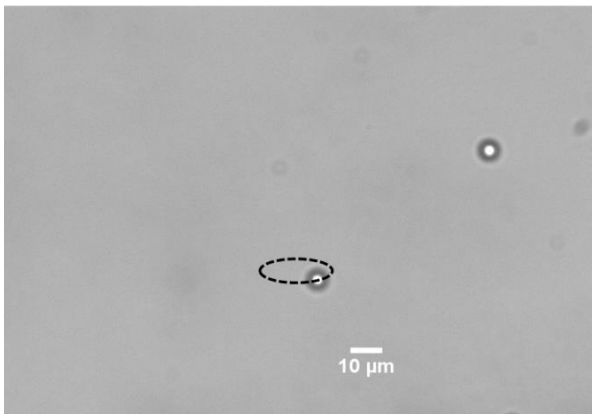

Figure 4.3.7 (g) Demonstration of the possible manipulation of the trapped particle. The trajectory of manipulation of the trapped particle is marked by black dashed line. The size of the polymer sphere was 3-micron. The trapped particle moves clockwise.

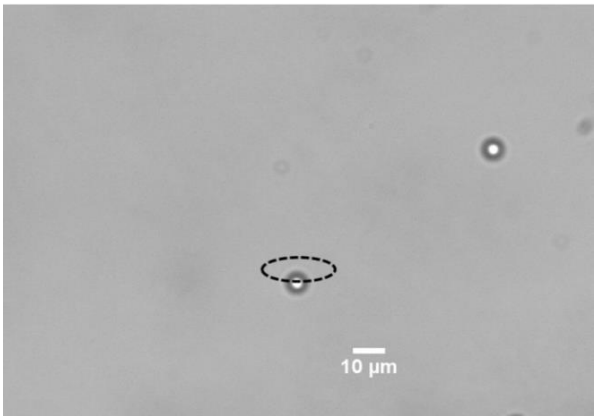

Figure 4.3.8 (h) Demonstration of the possible manipulation of the trapped particle. The trajectory of manipulation of the trapped particle is marked by black dashed line. The size of the polymer sphere was 3-micron. The trapped particle moves clockwise.

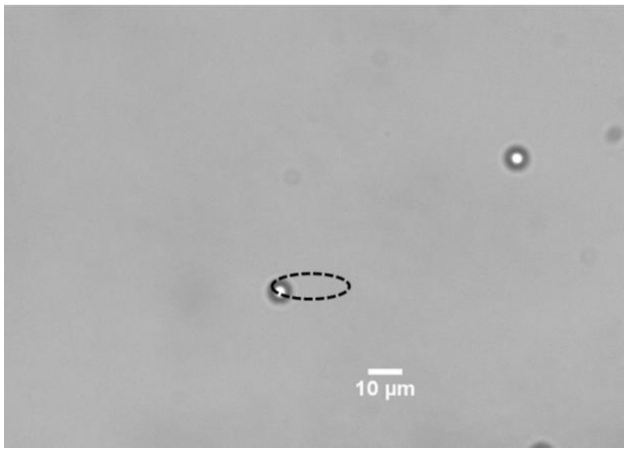

Figure 4.3.9 Demonstration of the possible manipulation of the trapped particle. The trajectory of manipulation of the trapped particle is marked by black dashed line. The size of the polymer sphere was 3-micron. The trapped particle moves clockwise. The trapped particle riches the same position as in case of (a).

Chapter 5

Trapping parameters

5.1 The method of estimation of trapping force.

5.2 Characteristic of trapping 1 micron polymer spheres.

5.1 The method of estimation of trapping force

Normally, the trapping force in laser traps is not measured directly. The trapping force can be determined by Hooke's law:

$$F = -\alpha x \tag{5.1.1}$$

Where F is applied force, α is the stiffness and *x* is a displacement.
The trap is characterized by trap stiffness, which is determined first. There are plenty of different methods for estimating the trap stiffness. In this chapter, we will explain the one we used for determining the trap stiffness.

The trap stiffness can be obtained through the **Equipartition theorem** by analyzing the thermal fluctuations of a trapped object. When the object is trapped in a harmonic potential:

$$\frac{1}{2}k_B T = \frac{1}{2}\alpha\langle x^2\rangle \tag{5.1.2}$$

Where α is trap stiffness, k_B is Boltzmann's constant, T is absolute temperature and x is the displacement of the particle from its trapped equilibrium position.

Then the stiffness can be obtained from the variance of displacements of the trapped particle from its equilibrium position, determined by $\langle x^2\rangle$ what is equal to the

integral of the position power spectrum. For the Equipartition method there is no dependence on viscous drag of the trapped particle.

Optical potential analysis comes out from the Equipartition method and instead of determining the variance of the distribution, the complete distribution of particles positions visited due to thermal motions is determined. The probability for the displacement of the trapped object in a potential well will be given by Boltzmann distribution [28]:

$$P(x) = \exp\left(\frac{-U(x)}{k_B T}\right) = exp\left(\frac{-\alpha x^2}{2k_B T}\right) \quad (5.1.3)$$

Where *U(x)* is the potential energy and $k_B T$ is the thermal energy.

The shape of U(x) is obtained from the normalized histogram of the particle positions:

$$U(x) = -\ln(P(x)) \quad (5.1.4)$$

It's common to use TEM_{00} Gaussian laser beam as a trapping beam, as it results in a harmonic trapping potential. For extracting the trap stiffness, the parabola $y = ax^2 + b$ should be fitted to the data of central region of the potential. Then the trap stiffness coefficient is:

$$\alpha = 2a/k_B T \quad (5.1.5)$$

The advantage of this method is that it gives the information about the potential in the region away from the trap center where the optical potential is non-harmonic [29].

5.2 Characteristic of trapping 1-micron polymer spheres

Applying different laser power, one micron polymer sphere was trapped and the fluctuations caused by the Brownian motion of the polymer particle in the trap were measured using position sensitive detector. Then the data was imported to the TweezPal software and the trap stiffness and other trap parameters were determined. Every optical setup of optical tweezers requires calibration before the trapping force can be determined. There are few methods for precise calibration and estimation of trapping force, but all of them require knowledge in programming languages such as MATLAB, IDL, LabVIEW. However, TweezPal software was proposed for quick, user friendly analysis and calibration of the optical tweezers. This software runs in the windows operating system and has a graphical user interface [28]. First, the Brownian motion of the particle in the trap should be detected. Then the data file should be imported to the TweezPal. Next, the trajectory, XY chart, position distribution histogram, trapping potential and trap anisotropy can be easily obtained. The trapping stiffness is determined from the variations of positions using Boltzmann statistics. Finally, the trapped stiffness is extracted from harmonic trapping potential.

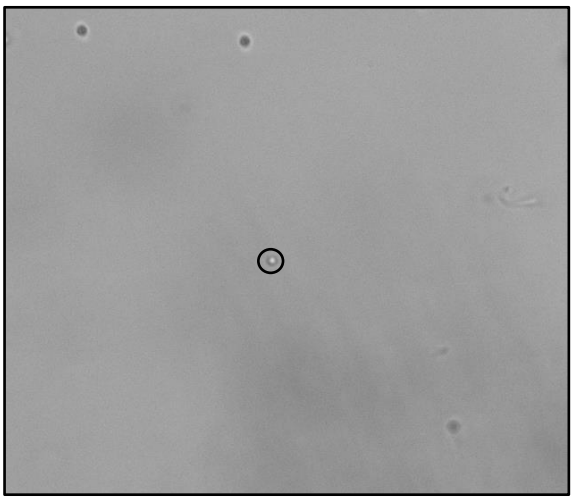

Figure 5.2.1 Demonstration of the trapping 1 micron polymer sphere. The 1 micron polymer sphere is marked by black circle.

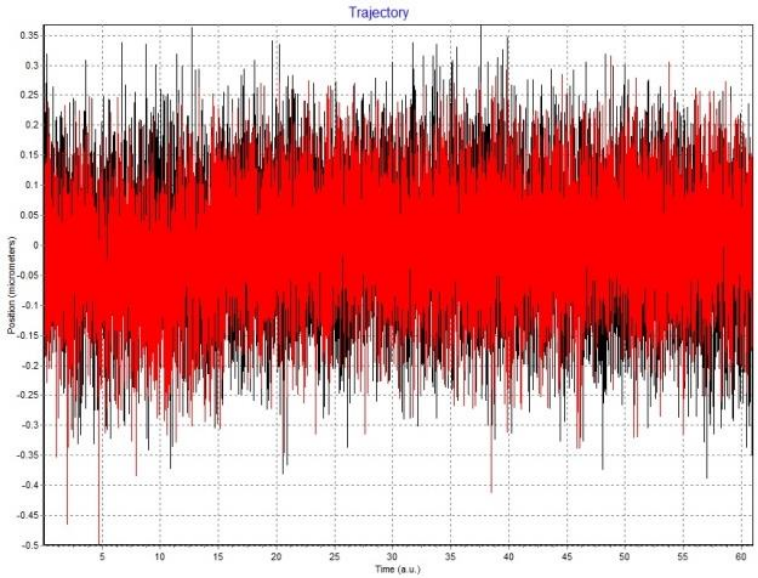

Figure 5.2.2 The trajectory of 1 micron polymer sphere while holding it in the trap. The black trajectory corresponds to x direction and the red one to the y direction.

Figure 5.2.1 shows the image of the trapping 1 micron polymer sphere in the water. Using position sensitive detector, the distribution of position of the polymer hold in the trap was obtained. The trajectory of the trapped polymer sphere is demonstrated in Figure 5.2.2. To understand if the polymer sphere was trapped symmetrically and in the centar of the focused laser spot, where the maximum intensity should be detected, we obtained the XY chart (Figure 5.2.3) and the trap anisotropy (Figure 5.2.4) of the 1 micron polymer sphere hold in trap. From these results we can understand that the polymer sphere is trapped in the center of the laser trap and trap in the region of the highest intensity.

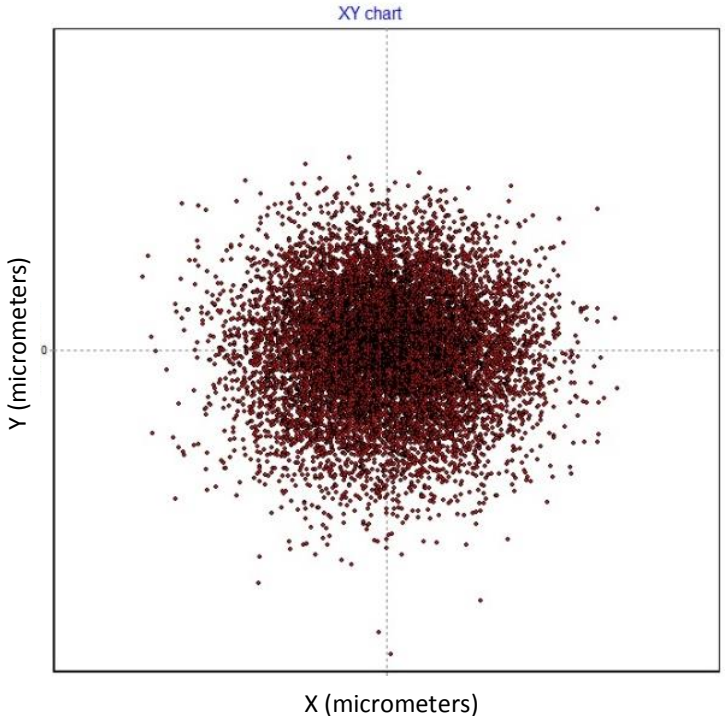

Figure 5.2.3 The XY chart of the 1 micron trapped polymer sphere.

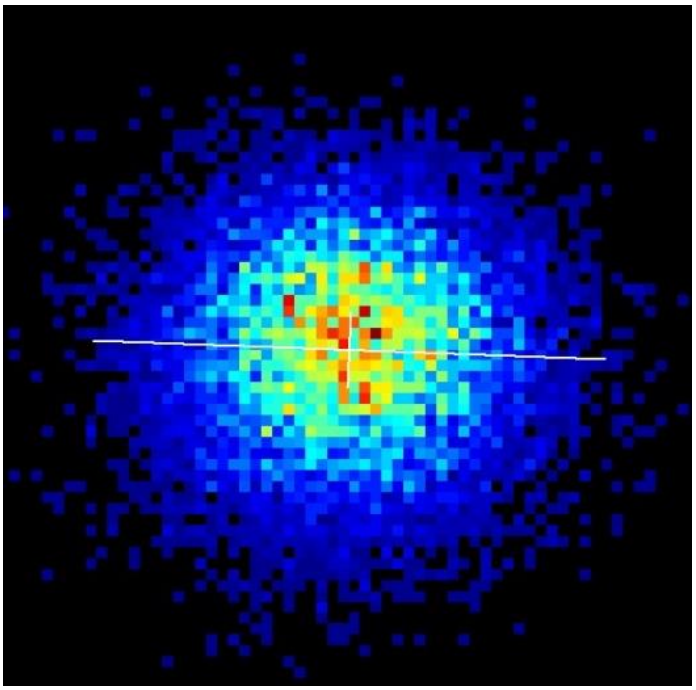

Figure 5.2.4 The trap anisotropy of the 1 micron polymer sphere.

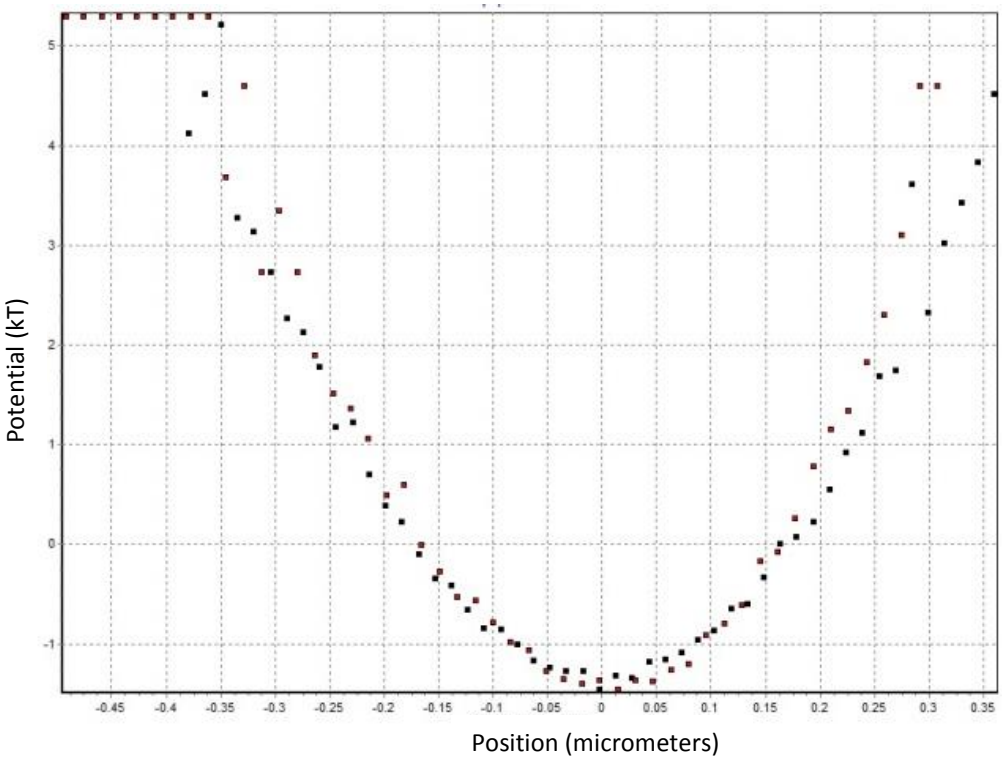

Figure 5.2.5 The trap potential of 1 micron polymer sphere for x and y directions.

The calibration of optical trap can be provided using Boltzmann statistics. In case of the particle is trapped in harmonic trapping potential, the optical tweezers are calibrated and then the force has to be found. The trapping potential is demonstrated in Figure 5.2.5. We fitted the parabola to the data in the central region of the potential and extracted the trap stiffness. The trap potential has a good shape and for both axes is very similar, what proves that the trapping force is strong in both directions.
At the Figure 5.2.6 the position distribution is shown, which shows that the distribution in the trap is quite similar in both directions and the shape demonstrates the peak which corresponds to the trapping in the center of the laser spot.

Next, we investigated the relationship between applied laser power applied and optical force determined from the trapping potential. The applied laser power varies from 3mW until 64mW as shown in Table 5.2.1. The smallest laser power required for optical trapping was less than 3mW, but the trapping wasn't stable enough and for the detection of trapped scattered light when less than 3mW was applied for trapping. In the previous chapter, it is discussed about trapping below 3mW.

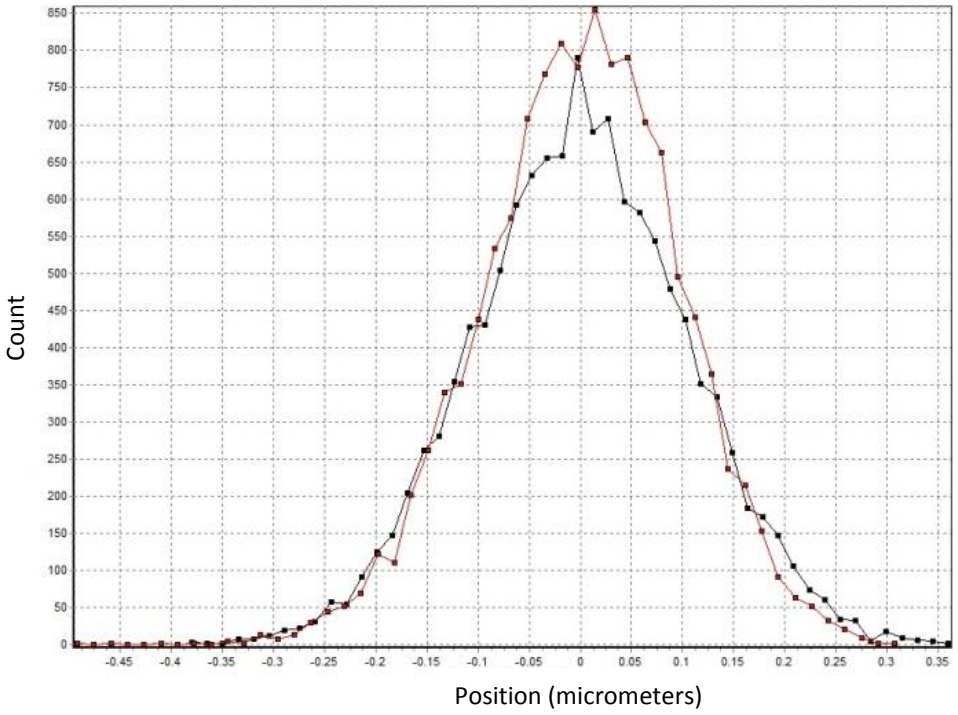

Figure 5.2.6 The position distribution histogram of the trapped 1 micron particle

Table 5.2.1 The trapping force depending on the applied laser power.

Laser power, mW	k_x, N/m	k_y, N/m
3.425	4.72E-08	7.01E-08
5.175	9.21E-08	1.41E-07
7.6	1.74E-07	2.55E-07
12.25	3.62E-07	4.36E-07
17	6.13E-07	7.77E-07
21.9	8.26E-07	9.43E-07
27	4.99E-07	6.94E-07
31.85	6.85E-07	8.98E-07
36.9	7.00E-07	1.06E-06
42.1	8.82E-07	1.26E-06
47.15	1.02E-06	1.48E-06
52.75	1.07E-06	1.74E-06
58.1	1.29E-06	2.08E-06
63.5	1.32E-06	2.42E-06

The dependence of the trapping force on the laser power was plotted and demonstrated at the Figure 5.2.7. With increasing the laser power, the trapping force increases linearly till the laser power stays almost 22mW. At this point due to Brownian motion one more polymer sphere came close to the trap and was trapped.

This results in decreasing the trapping force dramatically for a once. However, the trapping force continues increasing slower and the difference of the trapping in two directions increases much faster than for the trapping a single polymer sphere. The difference of trapping force in the x or y direction is caused due to not symmetric distribution of focal spot after objective of high numerical aperture. On practice, it is impossible to achieve an ideal symmetrical distribution and often it is not required and can be used as an advantage of trapping for specific tasks.

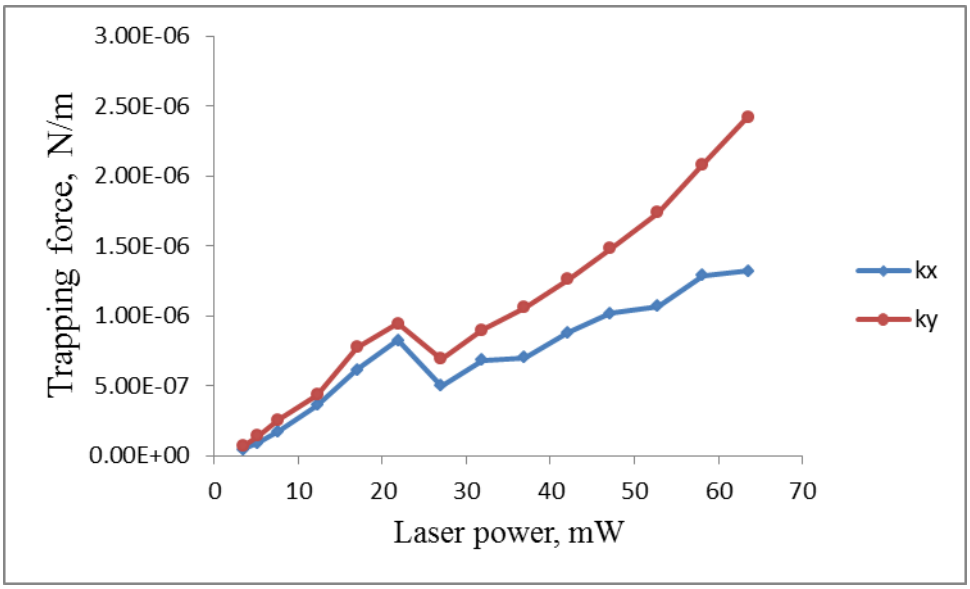

Figure 5.2.7 The dependence of the trapping force on the applied laser power.

Chapter 6

The method for measuring viscosity of liquids using laser trapping technique

6.1. Introduction

We applied laser trapping technique for measuring viscosities of liquids. The advantages of the applying this technique for viscosity measurements are:

- Requires small amount of examined liquid;
- Possible to obtain measurements in nonhomogeneous liquids;
- Applicable for biological cells, as it's a non-invasive technique;

The target of our work is to develop an optical technique for measuring viscosities of liquids with father applications for measuring and analyzing the viscosity inside

biological cells, cell elasticity and mechanical properties of the biological cells. Analyzing biological cell viscosity can be applied for the cell diagnosis and will provide a better understanding of the drugs delivery to the cell.

To achieve this goal we combined optical microscope with laser trapping technique and proposed the calibration method for determining the viscosity depending on the motion of the trapped particle in the liquid the viscosity of which have to be determined.

Optical trapping is a widely used technique in many applications such as Raman spectroscopy of singly trapped beads or biological cells [30, 31], photonic force microscopy with functional nanostructures [32], and the manipulation and assembly of nanotubes and nanoparticles. Various particles (e.g., atoms [33], gold and silver nanospheres [34], nanoparticles and quantum dots [35, 36], microscopic bubbles [34], and aerosol droplets [38]) can be trapped, manipulated, and assembled with optical tweezers while using laser microscopy to study the physical or biological processes. Optical tweezers are effective tools in mechanical and single molecule measurements [39], single cell and single molecule sorting [40], trapping and rotation of bacteria [41], the study of bacterial adhesion [42], and study of red blood cell aggregation [43]. Laser trapping can be combined with a variety of other optical techniques. For instance, the combination of optical tweezers with simulated emission depletion nanoscopy [44] has been reported. In that study, polymer particles were attached to both sides of a strand of DNA to trap and stretch the DNA. Six-fold resolution over confocal imaging was demonstrated. Another example of combination is 3D holographic optical tweezers with a spinning-disk confocal microscope for the study of the kinetics of cell division in yeast [45].

6.2. Experimental setup

We designed an experimental setup for analyzing the viscosity for the liquids, which has a limited access and volume. We combined an optical microscope with optical tweezers as demonstrated in Figure 6.2.1. The ability to use a microscope in the regime of not only light transmitted, but fluorescent allows us to visualize short distances of

movement of the fluorescent particles that are as small as 300 nm. The NIR laser ($Nd:YVO_4$) with a wavelength of 1064 nm was used to avoid the damage from the optical trap because the optical absorbance of biological tissues and cells is lower at wavelengths higher than the visible wavelengths [47, 48]. This plays an important role in the case of biological samples, as the absorption of laser radiation can damage the sample.

In our experimental setup, the trap was formed by tightly focusing the NIR laser with the objective lens of 1.4 NA and 60x magnification. The trapped particles were observed by imaging fluorescence or transmitted light on the CMOS camera. The trapped particle was manipulated by steering the laser beam with a galvo-mirror system (mounted XY Galvo set from GSI Lumonics, 010-3030015). For the observation of particles with sizes of a few hundred nanometers, the fluorescence was excited by a mercury lamp and dichroic mirrors and filters were used to block the excitation light. 35 mm petri dishes with 12 mm cover glass affixed to their bottom were used as a trapping chamber. This type of chamber enables high magnification and fluorescence observation under a microscope. The chamber for trapping was filled by the sample liquid.

The trajectory, amplitude, and the frequency of the movement of the trapped bead can be controlled by a galvo mirror system, as shown in the inset of Fig. 6.2.1. As a preliminary test, we trapped and manipulated 1-μm diameter polymer spheres. The trapped particles were moved along short distances of 5 μm. A major advantage of this technique is that, depending on the application, the distance and the direction can be changed. This provides the ability of measuring the dense and inhomogeneous space inside a cell.

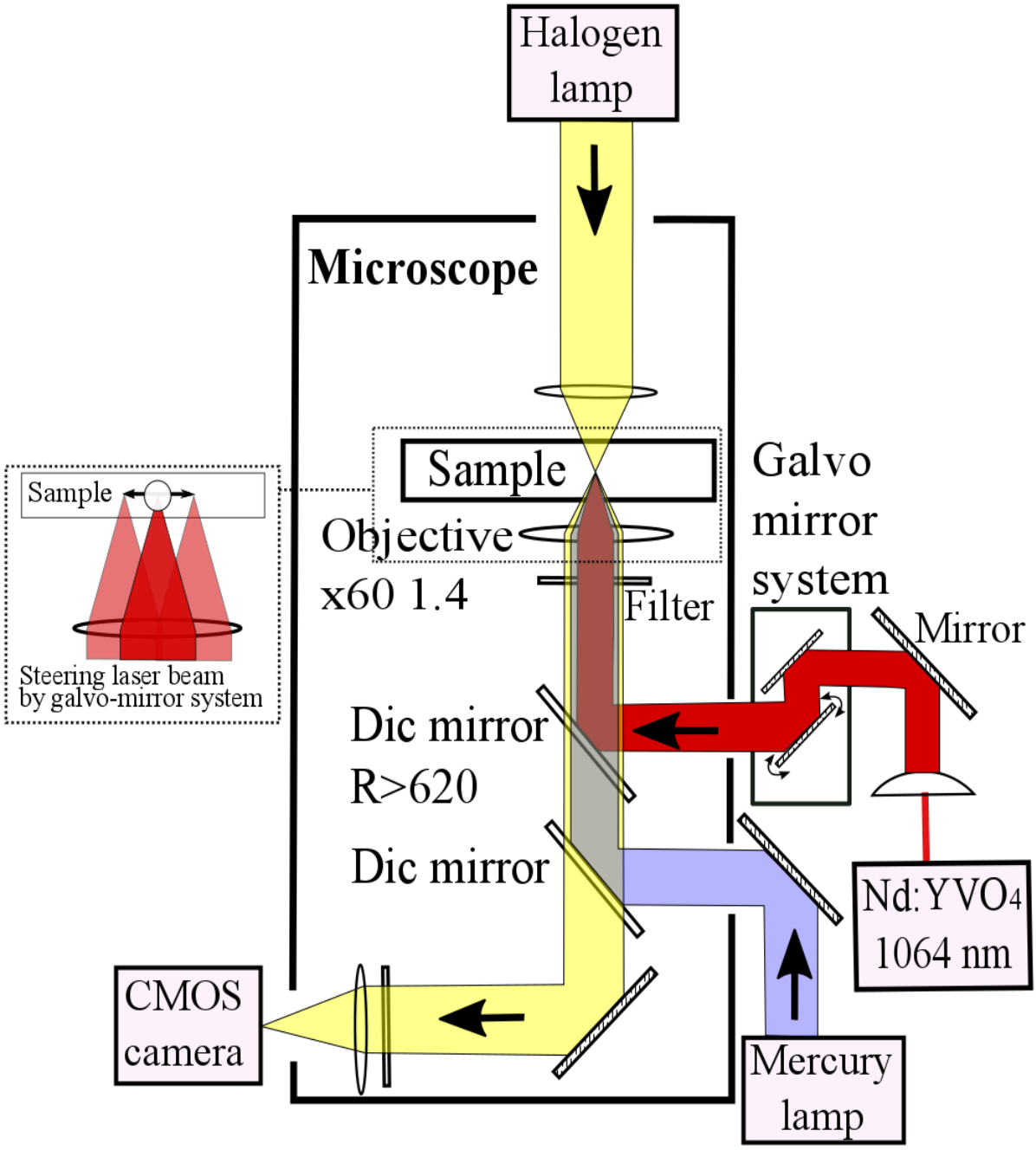

Figure 6.2.1. Optical setup based on combination of an optical microscope and optical tweezers. A Nd:YVO_4 laser was used for laser trapping. A mercury lamp was used for fluorescence imaging. DM, dichroic mirror.

6.3 Results

6.3.1 Dependence of particle displacement on the frequency of trap motion

For varying viscosity, water-glycerin mixtures were used. Glycerin is a well-studied Newtonian liquid with high solubility in water. In our experiment water-glycerin mixtures with concentration of 10, 20, 30 and 40% of glycerin were examined. 1-micron polymer spheres were immersed in the examined liquid placed into the Petri dish. Next, the laser beam was irradiated to the Petri dish and when the polymer sphere riches the region of the laser beam, it was trapped and manipulated with fixed amplitude, but with variable frequency, as shown on the Figure 6.3.1.1. When the frequency of the manipulation is enough low, the trapped particle follows the input amplitude of the laser beam. In the Figure 6.3.1.2, the displacement of the trapped polymer sphere with frequency 1 Hz is demonstrated. With increasing frequency, the amplitude of the manipulated particle decreased because of the drug force caused by the viscosity of the liquid. We want to investigate how fast the amplitude of the trapped particle decreases with increasing the frequency of the laser beam and how does it depend on the viscosity of the liquid to be trapped in. First, the amplitude dependence on the frequency of the trapped manipulated particle was investigated. Then the viscosity of the liquid was gradually increased and the dependence of the amplitude on the viscosity was obtained. Finally, we can plot the calibration curves for measuring the viscosity of unknown liquids.

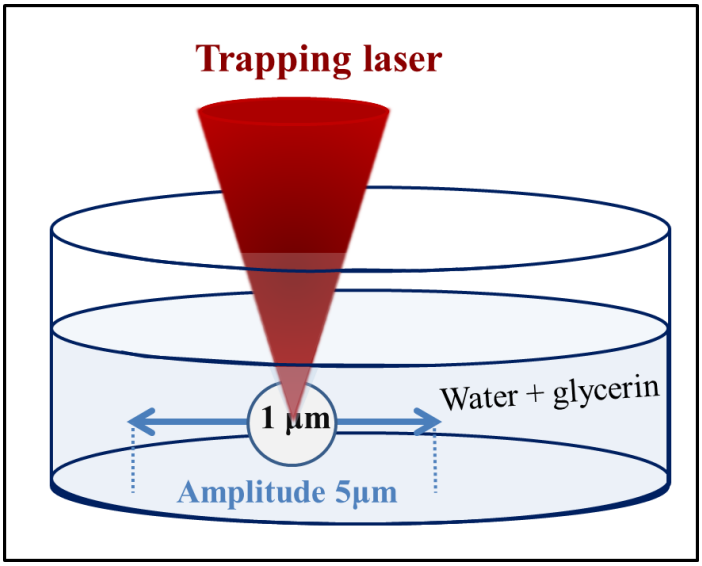

Figure 6.3.1.1 The demonstration of experimental details. The laser beam is marked by red, the trapped particle by white and the liquid to be studied is marked by blue. Blue arrow corresponds to the amplitude of laser beam. The trapped bead was 1 micron in diameter.

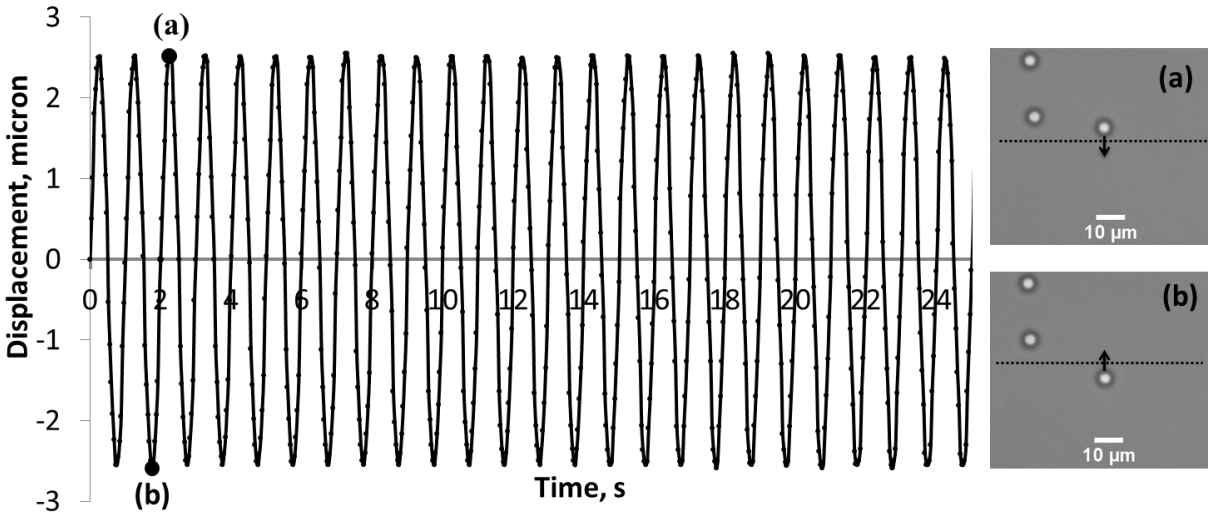

Figure 6.3.1.2 Demonstration of the trapping and manipulation of a 3-µm polymer sphere. The inset images show the position (a) and (b) of the trapped particle after manipulation, and black arrows indicate the displacement of the particle at the positions marked on the graph. The position of the trapped particle before manipulation is marked by the dashed black line.

The 1-µm polymer particles were trapped and manipulated in medium with unknown trapping properties. The position of the particle was detected by the camera and the video data was analyzed by Video Spot Tracker software [51]. We measured the displacement of a trapped particle in water-glycerin mixtures with 10%, 20%, 30%,

and 40% glycerin. Depending on the application, the size of the trapped bead can be decreased, but for that case new calibration should be provided

From Figure 6.3.1.3, we can see how the movement of the trapped particle depends on the applied frequency for the 1-μm polymer sphere trapped in water with various concentrations of glycerin. The amplitude of displacement of the trapped particle decreased with increasing frequency. For the increasing the frequency in the range of 1-4 Hz, the amplitude of displacement of trapped manipulated sphere remained constant. For frequencies above 4 Hz, the amplitude of displacement gradually decreased. The higher the concentration of glycerin, the faster the amplitude decreased with increasing frequency. In the case of 10% glycerin, the amplitude of movement of a trapped particle decreased more slowly than in the case of 40% glycerin. From the measurement shown in Fig. 6.3.1.3, we can understand that the displacement of the trapped particle decreases with increasing speed for various viscosities.

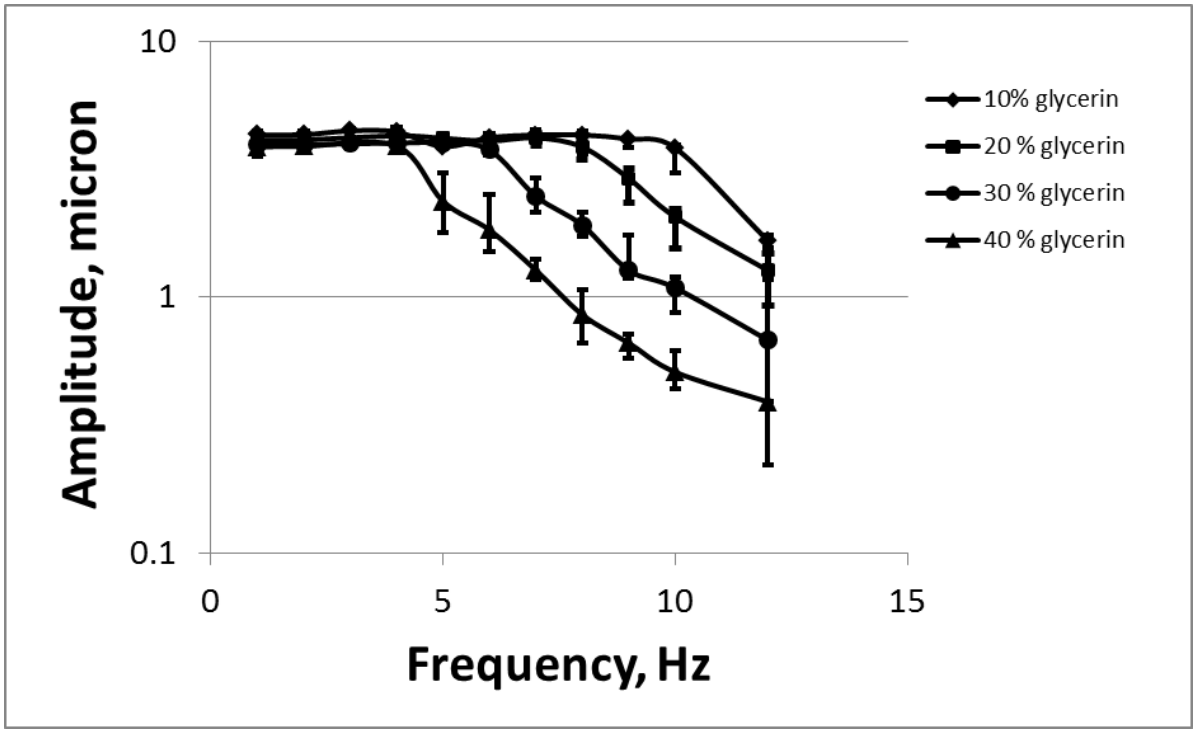

Figure 6.3.1.3 Measurements of the trapped particle displacement with increasing frequency and sample viscosity. Measurement were obtained for water-glycerin mixtures with 10%, 20%, 30%, 40% of glycerin.

6.3.2 Dependence of displacement of the trapped particle on the viscosity of the trapping medium

The Table 1 shows the obtained the viscosity values of the examined mixtures from the literature [49]. We plotted the dependence of the displacement of the trapped particle on the viscosity of the trapping medium at chosen frequencies.
To plot this dependence, shown in the Figure 6.3.2.1, we used the values of measured amplitudes obtained from the Figure 6.3.1.3 and the viscosity values from the Table 1.

Table 1 Viscosities for liquid solutions of glycerin and water.

Glycerin (% Wt.)	Viscosity (cP)
10	1.31
20	1.76
30	2.5
40	3.72

We chose the dependence of the amplitude on the viscosity for frequencies of 9, 10, and 12 Hz. Figure 6.3.2.1 shows plots for 9, 10, and 12 Hz for different concentrations of glycerin (10%, 20%, 30%, and 40%). From this graph, we can see how the amplitude of the trapped particle depends on the viscosity of the trapping medium. The proposed method covers the range of viscosities from 1 cP till 4 cP. We plan to measure viscosities of liquids in this range and we expect it to be enough for many biological samples. There are biological cells viscosities of which lie in the range of 1-3 cP. For example, cytoplasmic viscosity of epithelial cells (1.1-1.5 cP), cytoplasmic viscosity in CV1 and PtK1 cell (similar to that of water), fluid-phase viscosity of MDCK cells (near 1cP) and the sea urchin egg (2.3 cP) [50]. The matrix viscosity for HeLa is 1cP and for Swiss 3T3 cells is 0.88 cP [51]. The calibration for the high viscosity mediums can be provided if it’s necessary.

As expected, the displacement of the trapped particle decreased with increasing viscosity (increasing concentration of glycerin). To obtain the viscosity of an unknown liquid, we propose to measure the amplitude of a trapped particle at chosen frequencies and determine the corresponding value of displacement from Figure 6.3.2.1.

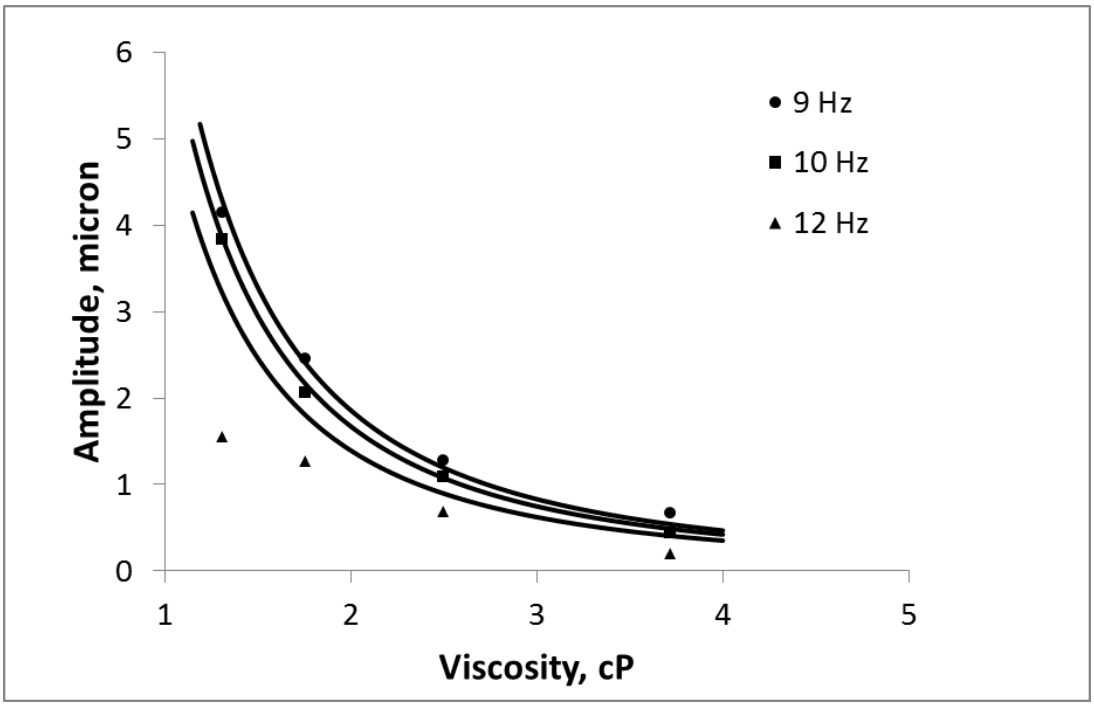

Figure 6.3.2.1. Dependence of the trapped particle displacement on the viscosity of the trapping medium. Measurements were obtained for the water-glycerin mixtures at an oscillation frequency of 12 Hz. The viscosity was varied by changing the concentration of glycerin.

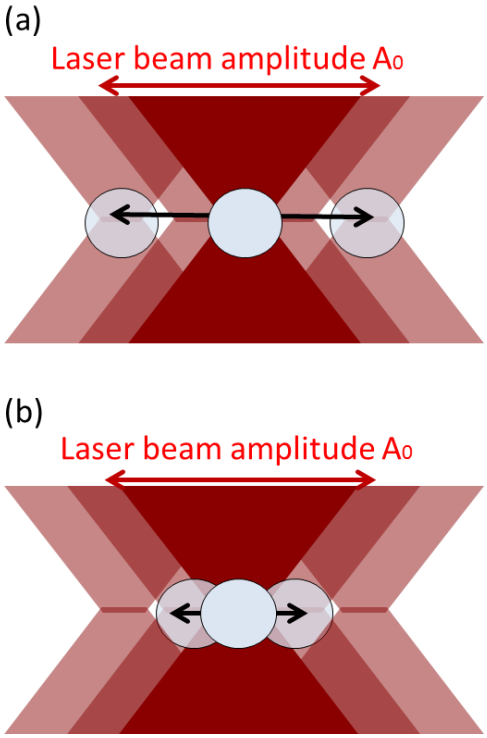

Figure 6.3.2.2 The oscillation of the trapped particle forced by laser beam. The trapped particle is marked by gray sphere and the black arrow corresponds to the output amplitude of the trapped particle. When the speed of the laser is enough slow, the amplitude of the motion of trapped particle follows the laser beam input amplitude (a). With increasing the laser beam speed, the amplitude of the motion of the trapped particle gradually decreases.

Motion of the trapped polymer sphere in viscous liquid due to the trapping laser can be explained in terms of a forced damped oscillator. In this case, the trapped particle oscillates in the viscous liquid. The motion of laser trap is treated as a force applied to the particle, while the dragging force in the viscous liquid corresponds to the dampening of oscillations. The schematic of the oscillation of the trapped particle is shown in Figure 6.3.2.2.

For our case, we can write equation of the damped forced oscillator as:

$$m\left(\frac{d^2x}{dt^2} + \alpha\frac{dx}{dt}\right) = F(t), \qquad (6.3.2.1)$$

where α is a viscous damping coefficient and $kx = 0$ because the natural frequency of oscillation is equal to zero. The applied force to the trapped particle is:

$$F(t) = A_o\, e^{-i\omega t},$$

where ω is the frequency of the trapping laser and A_0 is the maximum displacement of the laser beam.

The solution to equation (1) is:

$$x = Ae^{-i\omega t}, \qquad (6.3.2.2)$$

where x is the displacement of the trapped particle and A is the amplitude of motion of the trapped particle, which is given as:

$$A = \frac{A_0}{m\omega^2}\sqrt{\frac{1}{1+(\frac{\gamma}{\omega})^2}}\,. \qquad (6.3.2.3)$$

Because the damping of oscillations is due to the viscosity of the trapping medium, equation (3) can be simplified as:

$$A = \frac{\mathrm{K}}{\omega^2}\sqrt{\frac{1}{1+L(\frac{\eta}{\omega})^2}}\,, \qquad (6.3.2.4)$$

where K and L are constant parameters, and η is viscosity of the liquid.

Equation (4) was used as a fitting function of the experimental data shown in Fig. 5. For the case of 12 Hz, the experimental data did not match the theoretical curve; for this frequency, the displacement decreased much faster and for higher frequencies the detection of small displacement by camera gives higher error of measurement. The curves in Fig. 6.3.2.1 can be used as a reference curves. If we know trap particles in a liquid with unknown viscosity, we can measure the motion for frequencies of 9 or 10 Hz. Then, from Fig. 6.3.2.1, the measured displacement of the trapped particle can be compared to estimate the unknown viscosity value.

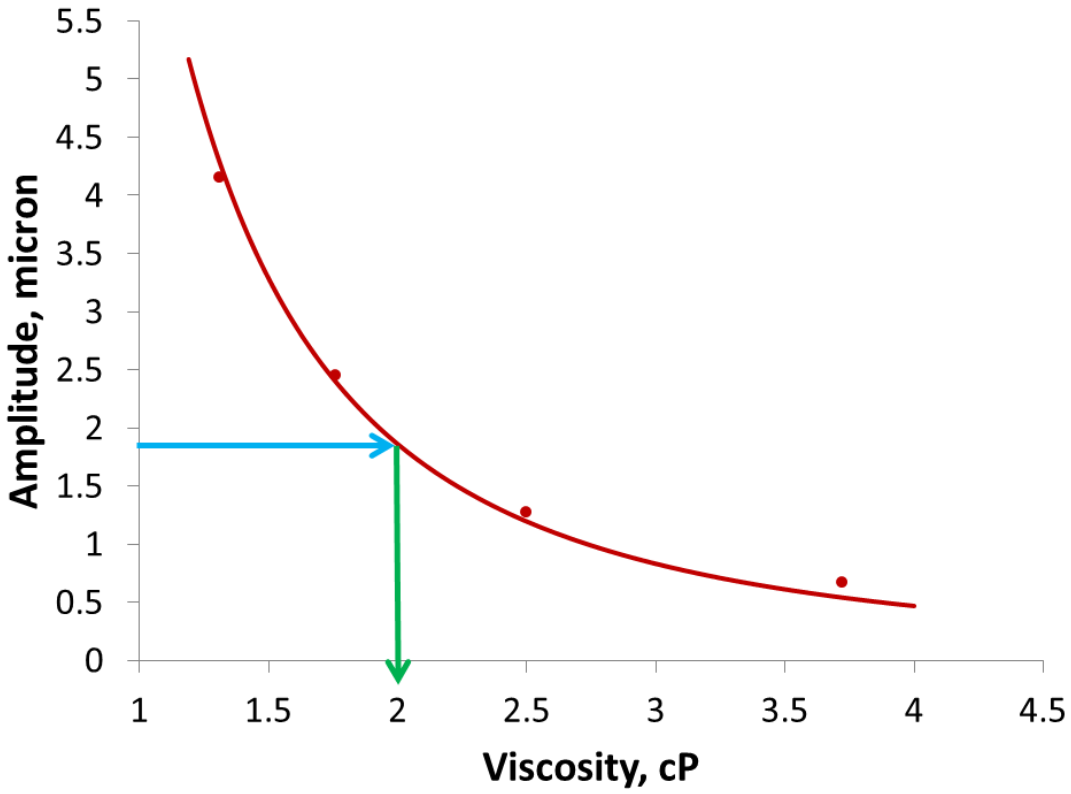

Figure 6.3.2.3 The example of the measuring the viscosity of the propanal by proposed method. Blue arrow corresponds to the measured amplitude of the motion of the trapped polymer sphere in propanol at the laser frequency of 9 Hz. The green arrow shows the value of viscosity which corresponds to the measured amplitude.

Finally, for the confirmation of proposed curves we trapped the 1-micron polymer sphere in 2-propanol. Then the particle was manipulated with frequency 9 Hz in 2-propanol and the amplitude of motion was measured. Then from proposed calibration curve for 9 Hz, we can find the value of viscosity, which corresponds to the measured amplitude, as shown in the Figure 6.3.2.3.

Next, we compared the theoretical viscosity value of the 2-propanol with the experimentally measured viscosity value. The experimentally measured value was 2.00cP, what is in good agreement with the theoretical value of 2.04cP.

6.4. Conclusion

In summary, we have constructed a setup to optically measure liquid viscosity by combining optical tweezers with optical microscopy. By analyzing the movement of the trapped particle in water-glycerol mixtures, we observed that the displacement of the trapped particle decreased with increase in the viscosity of the water-glycerol mixture. To explain this dependence, we proposed a forced damped oscillator approach. By knowing this dependence, we are able to apply it for measuring viscosities of unknown mixtures. To measure viscosity, we need to measure the amplitude of movement of the trapped 1-μm diameter polymer bead at chosen optimal frequencies (9, 10 Hz), and then find the corresponding value of viscosity in Fig. 6.3.3.2. We have tested our proposed reference curve for estimation of 2-propanol viscosity.

As a future work, we plan to trap and analyze the movement of particles inside a biological cell. As biological cells can actively take up particles, it is important to find the optimal conditions for trapping particles inside the biological cells, e.g., the optimal size and material of the trapped particle, acceptable concentration, and laser illumination.

By measuring the trapped motion at chosen frequencies, we can estimate the viscosity inside a biological cell and provide a viscoelastic analysis. This novel diagnostic can be applied for medical diagnosis of the biological cells, as the movement of the trapped particle might depend on the state of the cell. For instance, there is a lack of techniques to measure the changes in the cellular hydration state. The cell hydration plays an important role in the regulation of the cell function, as a separate and potential signal for understanding cellular diseases [55]. Another possible application is probing the cell elasticity. It was reported that targeting the macrophage elasticity helps to determine innate macrophage function and may lead to novel treatments for human diseases [56]. The optical tweezers technique combined with microscopy will open new possibilities for controlling the location of particles for intracellular labeling. This technique can also be applied for investigations of intracellular transport mechanisms through cellular uptake of the nanoparticle.

Chapter 7

Applying laser trapping technique for measuring mechanical properties of the biological cells

7.1 Introduction

Cell functions are determined by cell structure, which differs depending on cell process. For example, understanding mechanic respond of the cell plays an important role in cell mechanics, as the intra cellular changes correspond to mechanical changes of the cells. It was reported that there is a biochemical response to the deformations of cells. Defects in the cytoskeleton may increase the fluctuation amplitude as well as induce shape changes [57].It was also reported that targeting the macrophage elasticity helps to determine innate macrophage function and may lead to novel treatments for human diseases [58].

Atomic force microscopy (AFM) is a widely-used technique for studying mechanical properties of the biological cells. AFM is high resolution technique for obtaining mechanical, electrical and magnetic characteristic samples. The basic AFM technique for quantitative study of mechanical characteristics of cells and tissues is the force spectroscopy, by recording the force value and vertical deflection of the

cantilever, the probe approaches the surface under the study at the fixed point and usually performs force-curve analysis. The force value versus distance between the probe and the surface can be plotted in this case [56]. On the other hand, conventional AFM tips are very sharp, which results in high local stress on the cell. Also, the lowest force is limited by the thermal noise of the AFM cantilever in liquid which limits the accuracy at which the absolute cell indentation can be measured [60]. Investigations of cell parameters will help to understand cellular processes better and to detect diseases easily.

7.2. Experimental setup

We combined optical microscope with optical tweezers as shown in Figure 7.2.1. For trapping and detection NIR laser with wavelength of 1064 nm was used. The displacements of trapped particle were controlled by scanning galvo mirror system (Thorlabs, GVS012/M).

For detection, we used back focal plane interferometry technique. In this case the trapping light can be used directly to detect small displacements of the trapped particle with high resolution. Depending what magnification of the detected signal can be used, the diffraction-limited resolution can be exceeded. For example, if the detected signal is magnified 1000 times, the 1 micron displacement can be detected as 1mm.

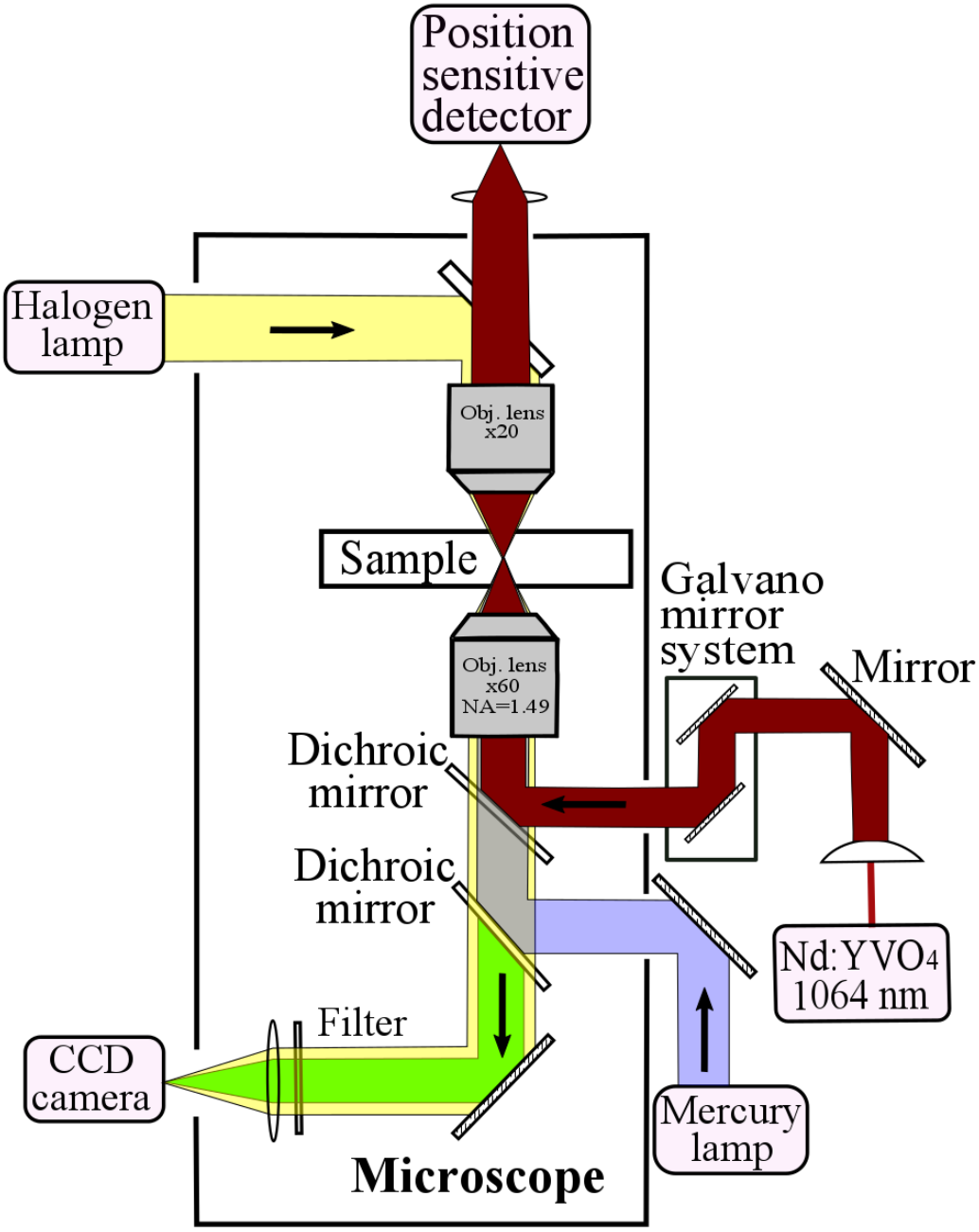

Figure 7.2.1 Optical setup of laser trapping. Nd:YVO_4 used for trapping and detection.

For probing cell elasticity, cancer cell named HeLa cell were grown. HeLa cells were cultured in Dulbecco's Modified Eagle Medium (DMEM) with 10% of Fetal Bovine Serum (FBS) using Petri dishes for 3 days.

7.3 Results

Before probing the cells, 0.5-μm fluorescent polymer spheres were immersed in the medium with HeLa cells. In order to confirm which object was trapped and what the displacement of the trapped sphere is, fluorescent spheres were used. Reflected and fluorescent image were observed simultaneously, allowing observing trapped florescent polymer spheres and HeLa cells without dyeing what is harmful for cells. Figure 7.3.1 demonstrates the indentation of HeLa cell with fluorescent polymer sphere. First, polymer sphere was trapped away from the cell and manipulated with amplitude of 3.2 micron as shown by white dashed arrow at the Figure 7.3.1 (a). Than in order to displace the trapped sphere close to the cell, the stage with sample was moved till the moving trapped polymer sphere was close enough for indention the cell. Finally, the indentation was detected using position sensitive detector. The frequency of the movement of trapped bead was 1 Hz. The distortion of the signal corresponds to the indentation and stretching cell.

While the indentation of the biological cell by polymer sphere different cell response occurred. For some cases, the cell was successfully intended, for some cases the trapped particle was stuck to the surface of the cell, after what the indentation and trapping was lost, but for some cases the trapping wasn’t lost and the cell was stretched by the stuck particle before it was detached from the cell membrane and continuously manipulated by laser trap. For some cases the particle stayed stuck to the cell membrane and was stretched by the polymer sphere while manipulation of the trapped particle. All of these cases are important in determining the mechanical properties of the cell, which will give the information about the functions and structure of the cells.

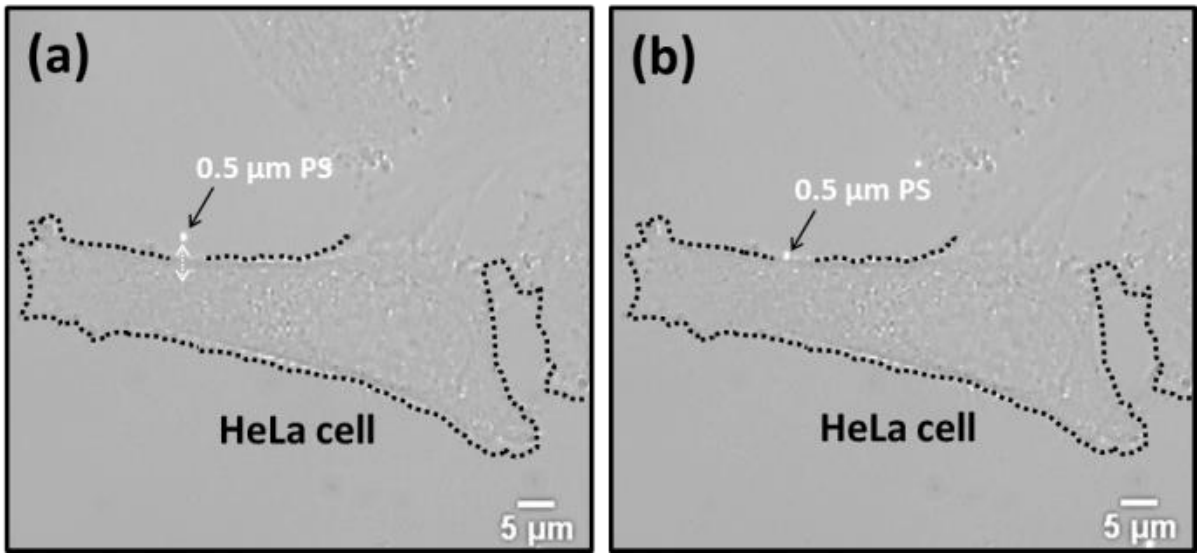

Figure 7.3.1 Hela cell indention with 0.5-µm trapped fluorescent polymer sphere. The membrane of the Hela cell is marked by black dashed line. The white arrow corresponds to the input amplitude of the laser. (a) Trapped polymer sphere before indentation of the cell membrane. (b) Trapped polymer sphere while indentation of the cell membrane.

For detection of the displacement of the manipulated polystyrene sphere, we used back focal plane interferometry technique. In this case, the trapping light can be used directly to detect small displacements of the trapped particle with high resolution. The diffraction-limited resolution is exceeded when the detected signal is magnified before being focused on the detector. For example, if the detected signal is magnified 1000 times, the 1-micron displacement can be detected as 1mm.

First, we will discuss the case when the trapping of the particle is lost while indentation of the cell, the schematic process of what is shown in the Figure 7.3.2. The polystyrene sphere was trapped (a), and moved to the surface of the cell (b). While indenting the cell (c-d), polystyrene sphere was lost from the trap (d). Thus, after indentation the laser beam was moved back away from the cell without trapped polystyrene sphere. We consider there are few reasons why the trapping can be lost. First, the depth of the indentation is very small compare to the maximum of the divergence of the applied laser beam amplitude. Thus, while indenting the cell membrane, there will be a moment of maximum possible indentation and the polystyrene sphere for the corresponding trapping force and the polystyrene sphere will be stopped by the cell membrane. It happens due to the laser beam divergence

on the distance far from the possible indentation distance, as the trapped particle will be not in the region of the laser spot and the trapping will be lost.

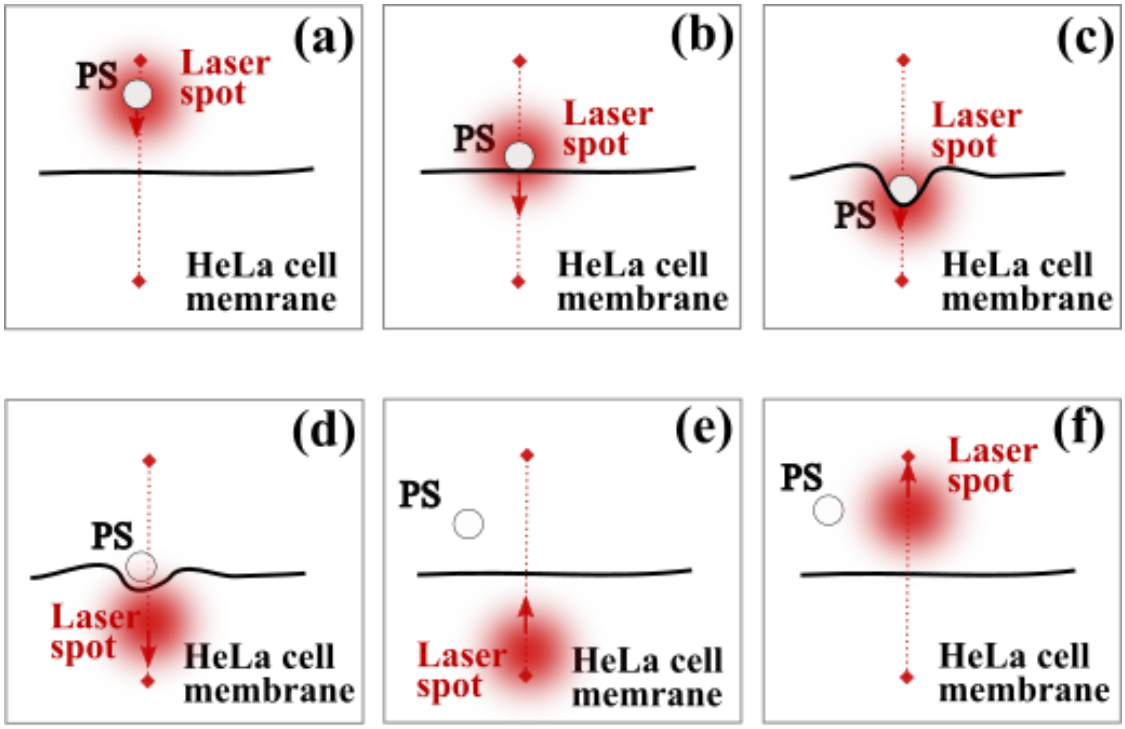

Figure 7.3.2 The schematic of the process of the indentation of the HeLa cell membrane for the case when the trapping is lost. Red spot corresponds to laser spot, white sphere to the polystyrene sphere (PS), red dashed line to the amplitude of the laser beam manipulation.

Next, we will discuss about the successful indentation of the cell. Figure 7.3.3 shows the schematic of process of the successful indentation of the cell. First, the polystyrene sphere was trapped around the cell membrane (a), moved closed to the cell membrane (b) and then the cell was indented by the trapped polystyrene sphere (c), after what the trapped polystyrene sphere was moved away from the cell membrane (d).

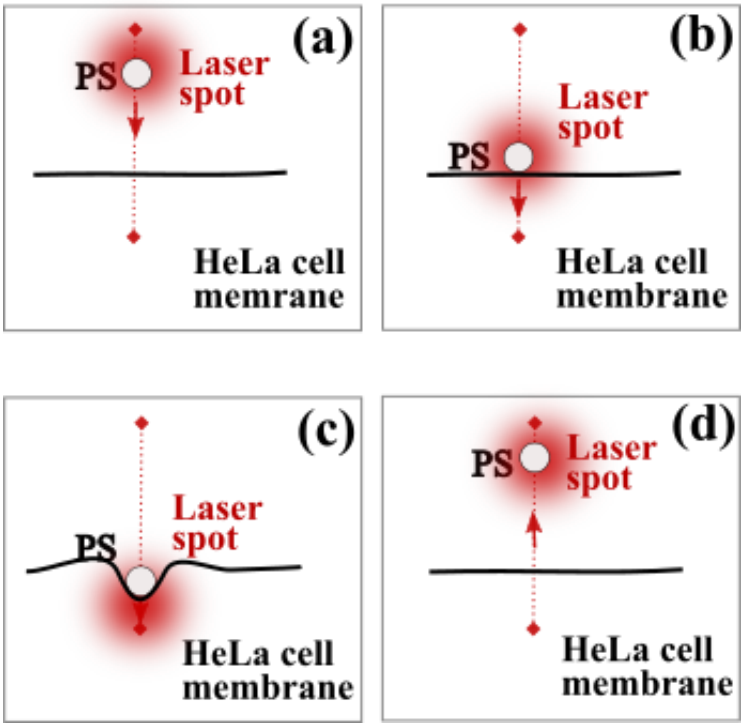

Figure 7.3.3 The schematic of the cell membrane indentation by polystyrene sphere. Laser spot is marked by red spot and polystyrene sphere is marked by white sphere. Red dashed line corresponds to the amplitude of the manipulation of the laser beam.

Figure 7.3.4 shows the result of indentation of the HeLa cell by trapped 0.5 fluorescent polymer sphere. The red curve corresponds to the displacement of the trapped polymer sphere while intending the cell. The blue curve corresponds to the displacement of the trapped bead in medium while not intending the cell. As a result, from Figure 7.3.2 we can understand the value of indentation of the cell by the trapped 0.5-micron polymer sphere. The distance marked by black arrow corresponds to indentation. When the sphere touches the membrane of the cell, the detected signal changes, as the time delay occurs.

Another example of probing cell is shown in the Figure 7.3.5. In this case, the cell was indented by trapped 0.5-micron polymer sphere, after what the sphere was stuck to the membrane, what caused the stretch of the cell and then the recovery of the cell membrane before the trapped particle was detached from the membrane of the cell. Thus, two peaks appeared while probing the HeLa cell by manipulated trapped bead. For the more detailed explanation, let us demonstrate how the indentation occurs in this case.

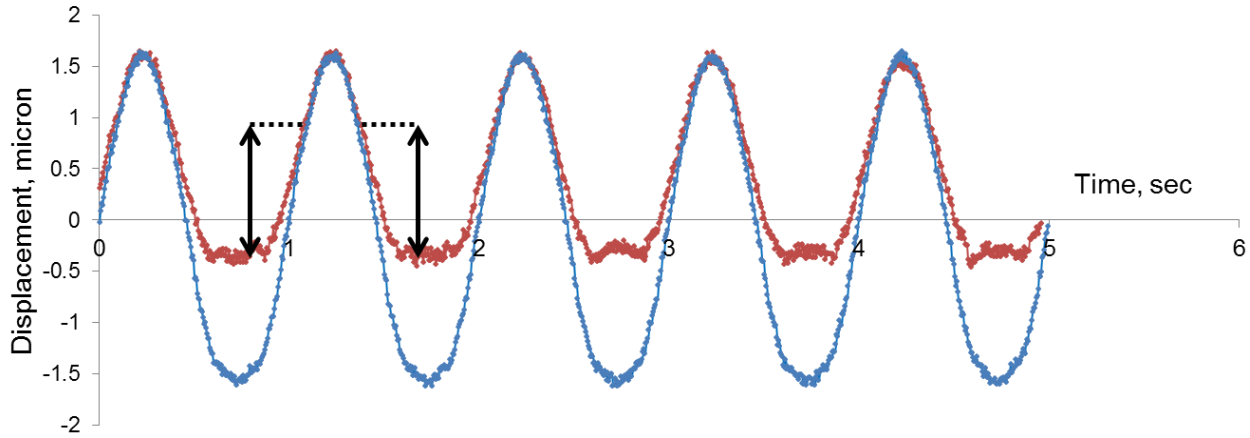

Figure 7.3.4 The displacement of the trapped manipulated polymer sphere in the medium while probing HeLa cell (red curve) and while not probing HeLa cell (blue curve).

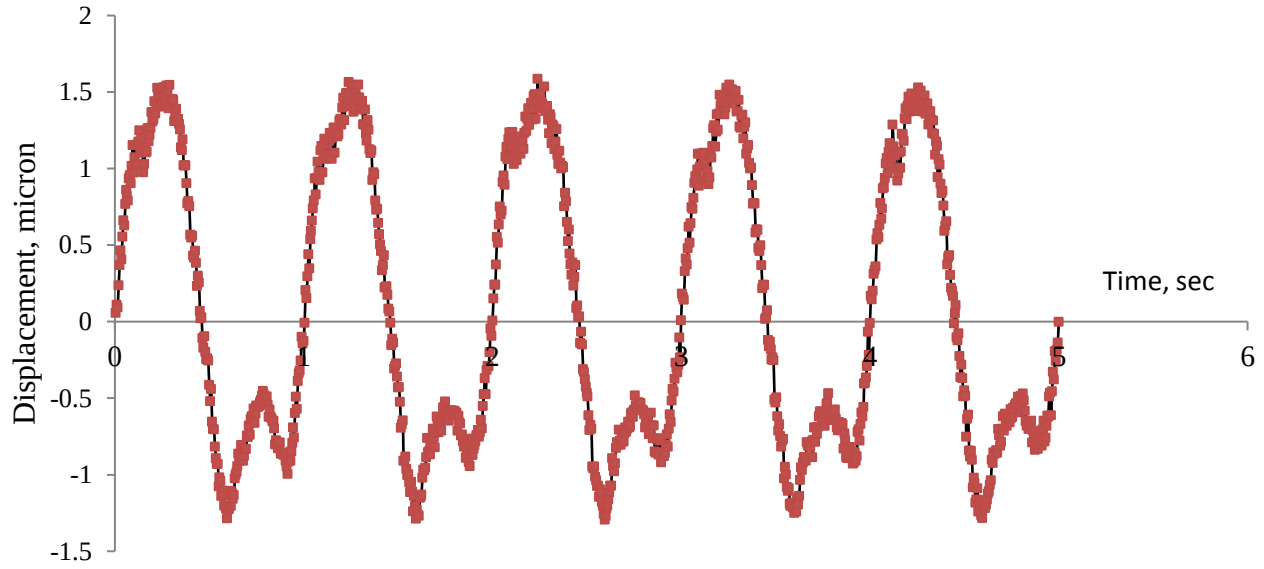

Figure 7.3.5 The indentation and stretching of the HeLa cell with 0.5-μm trapped fluorescent polymer spheres.

The Figure 7.3.6 explains the process of indentation of the HeLa cell occurs. First, polymer sphere was trapped and moved in the direction of cell membrane (a) until the trapped polymer sphere is above to push the membrane of the HeLa cell (b), then HeLa cell membrane is indented by trapped polymer sphere as shown in Figure 7.3.6 (c). While the cell membrane was recovering, polymer sphere was pushed by the cell membrane (d) which corresponds to the peak of the detected signal. However, the polymer sphere was stuck to the membrane of the cell that caused the cell stretch (e) till the trapped sphere could be disconnected from the membrane (f).

Before that happens, as a respond to the stretch, the cell slightly moved back, opposite to the direction of the stretch, pulling the polymer sphere (e) in the direction opposite to the laser beam motion. That explains a second minimum at the detected signal. As the laser spot was approximately twice bigger than the size of the particle and the displacement of the particle was within the laser spot, the trapping wasn't interrupted, the trapping might occur not at the maximum intensity of the laser spot. Finally, by measuring the depth of indentation and length of the stretched area of the cell we can estimate the elasticity of the HeLa cells. Figure 7.3.7 shows the example of the

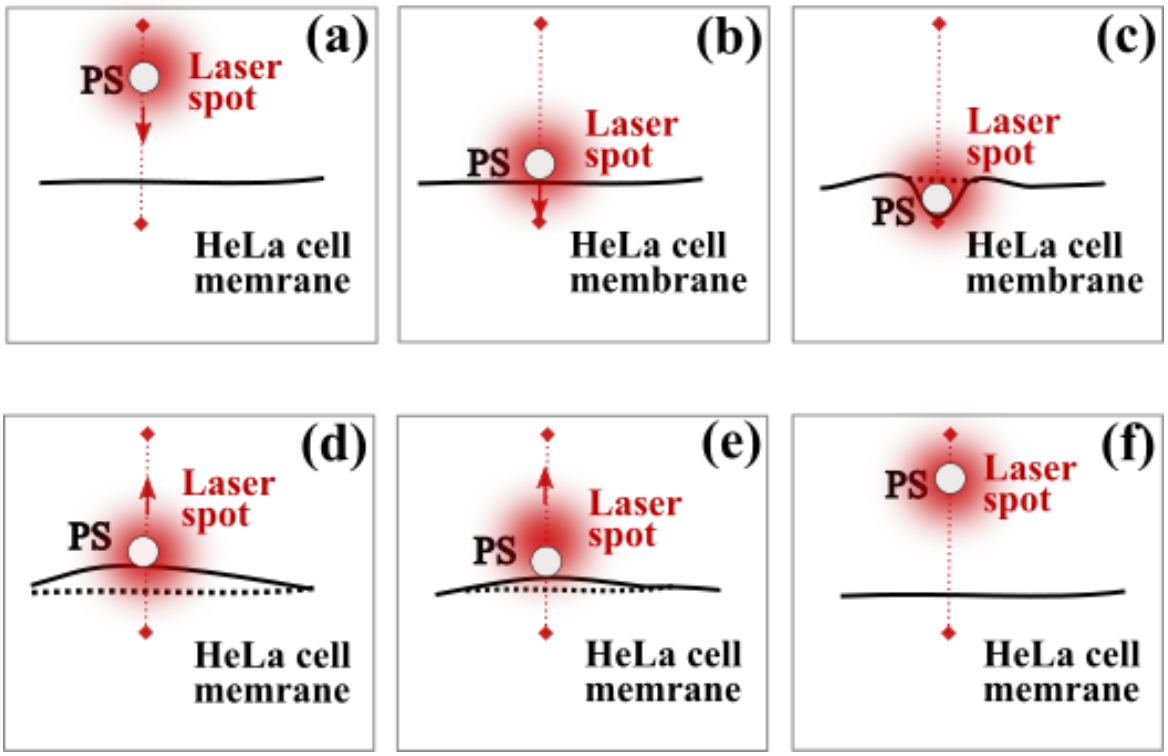

Figure 7.3.6 Scheme of the process of the indentation of HeLa cell. The focused laser spot is marked by red gradient circle sphere the maximum intensity in the center. The red arrow indicates the direction of the laser beam. The red dashed light line corresponds to the input amplitude and trajectory of the laser steered by scanning galvo mirror system. The 0.5-μm polymer sphere (PS) is marked by white sphere. The dashed black line shows how the shape of HeLa cell membrane changes compare to the previous image. Polymer sphere was trapped (a). Polymer sphere is moved to the membrane of the cell (b). The cell membrane was indented with PS (c). Stretching the cell by trapped polymer sphere stocked to the cell membrane (d). The trapped PS was slightly pulled back by HeLa cell (e). The trapped PS was moved away of the cell membrane (f).

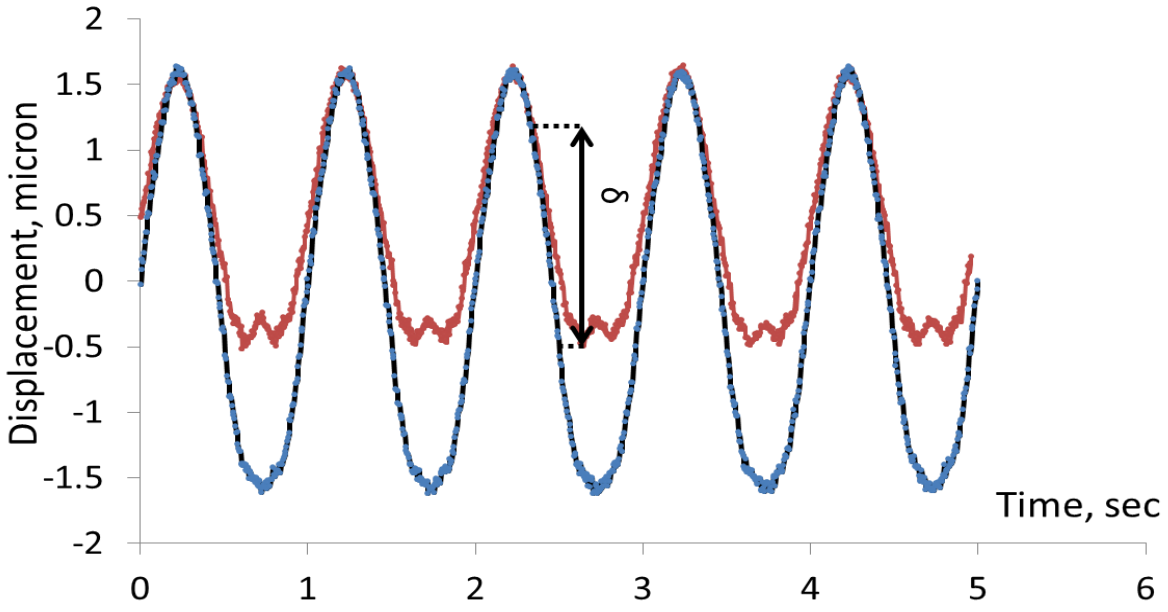

Figure 7.3.7 The displacement of the trapped manipulated polymer sphere in the medium while probing HeLa cell (red curve) and while not probing HeLa cell (blue curve).

displacement of the trapped manipulated polymer sphere in the medium while probing the cell for this case. The indentation δ can be determined from the Figure 7.3.7. When the polystyrene sphere starts indenting the cell, the time delay occurs, thus the depth of indentation can be determined.

To determine cell elasticity, the variation on the Hertz model was used. This model describes a deformation of a large elastic body with a disc shaped contact area. The relationship between applied force *F* and the resulting indentation *δ* is [58]:

$$F = \frac{4ER^{1/2}\delta^{3/2}}{3(1-\nu^2)} \qquad (7.3.1)$$

E- Young's modulus, *v*-Poisson's ratio of the indented material, *R*- radius of the rigid indenter.

From the equations (7.3.1) Young's modulus:

$$E = \frac{F*3(1-\nu^2)}{4R^{1/2}\delta^{3/2}} \qquad (7.3.2)$$

The trap force was obtained through the Equipartition theorem by analyzing the thermal fluctuations of a trapped object. Optical tweezers analysis and calibration software TweezPal was used for determining trapping force. First, the polymer sphere was trapped and the Brownian motion was detected using position sensitive detector, then the particle trajectory is imported into the software for calculation position histogram, trapping potential, stiffness and anisotropy. This software provides the quick analysis and calibration of the optical tweezers.

The trapping force was found from Hooks law and is proportional to the stiffness of the trap. The average indentation of the cell was 1.18 micrometers and the trap stiffness for 0.5-micron polymer sphere is: 4.15×10^{-4} N/m. Finally, using equation 7.3.2 we calculated the Young's module of the HeLa cell, which was 49.7kPa in case of experiment demonstrated at the Figure 7.3.4. Depending on the cell size and thickness and place to be indented we could sense the elasticity in the range of 26.5 - 49.7kPa.

7.4 Viscous drag force in comparison with trapping force

In our experiment, while obtaining the elasticity of the Hela cells, we neglected the viscous drag which acts on the trapped manipulated polystyrene bead. We discuss about impact of viscous drag compare with trapping force used in our experiments.
Reynolds number is the ratio of intentional forces to viscous forces within a fluid, and can be written as follows:

$$Re = \frac{\rho v L}{\mu} \tag{7.4.1}$$

where ρ is density of the fluid, v is velocity of the fluid with respect to the object, μ is a dynamic viscosity of the fluid.
We trapped the 0.5μm polystyrene sphere and indented the cell by it. From the detected cell response, we estimated the elasticity of the cell. For the cell elasticity

estimation, we neglected the drug force, which acts on the trapped bead, as it was only 4.43% of the trapping force.
For the experiment for estimating the cell elasticity, the polystyrene bead sized 0.5 micrometer in diameter and immersed in culture medium with viscosity closed to water the Reynolds number calculated using equation (1) is:

$$Re = 0.32 \cdot 10^{-8}$$

If the Reynolds number is very low($Re \ll 1$), the relationship between the force of motion is given by Stoke's law:

$$F_{drag} = 6\pi\mu Rv \qquad (7.4.2)$$

where μ is a dynamic viscosity of the fluid, R is a radius of the bead, v is velocity of the fluid with respect to the object.
The bead was manipulated with frequency 1Hz and the amplitude 3.2 micrometer, thus the speed of the manipulated polystyrene bead was 6.4μm/sec.
The drag force for the case when the trapped polystyrene bead indents the biological cell is:

$$F_{drag} = 0.03 \cdot 10^{-12} N$$

For the elasticity experiments, the trapping force for the 0.5-micrometer bead was:

$$F_{trap} = 13.28 \cdot 10^{-12} N$$

As a result, the viscous drag force is 4.43% of trapping force and can be neglected. However, while slightly increasing the laser power, the trapping force will increase dramatically and the viscous force will become even smaller compare to the trapping force. Thus, if we want to decrease the impact of the viscous drug force, we have to increase the laser power. For the cell elasticity measurements, the laser power was just around 20mW and as the laser beam is focused to the polystyrene bead, not directly to the cell, we can increase the laser power and the proposed technique still

will be non-distractive. As we use the high numerical aperture lens, the laser beam below the focal plane of the lens will be scattered very strongly and the amount of the light absorbed by the surface of the cell is very small and will not damage the cell.

7.5 Conclusion

It is proposed to apply the developed optical setup for the studying mechanical properties of the biological cells. To measure the elasticity of cells, we intend the cell by the trapped polymer sphere and study the response of the cell. The response of the cell differs; sometimes the trapped particle is stuck to the cell and then stretched before been detached from the membrane of the cell by laser trap, sometimes the indention achieved successfully and the respond of the cell is measured. The Young's module of HeLa cell is determined by applying Hertz model. The measured value depending on the cell size and thickness and place to be indented was in the range of 26.5 - 49.7kPa, which is reasonable value [60]. We believe that when the trapped particle is stuck to the cell or even the stretching of the cell by trapped particle occurs, it can give the additional information about the mechanical properties of the cell. Finally, we would be able to understand the functions of cell better and to apply it for cell disease treatment.

Chapter 8

Overview and future plan

The laser trapping is a promising technique for wide range of applications especially for investigations of biological cells. Laser trapping is a non-invasive technique and by controlling such parameters as wavelength of the trapping laser and the size and material of the trapped object, it is possible to achieve the desired application of laser trapping. The ability to trap and isolate or manipulate particles opens new abilities for improving existed research approaches or even creating new research approaches.

We have developed a new approach for measuring viscosities of liquids. It is applicable for obtaining measurements in the small volumes of liquids, which have a limited access or amount. We have obtained the relationship between the viscosity and the displacements of the trapped manipulated sphere. Thus, we can determine the viscosity of the liquids by knowing the displacements of the trapped particles in the liquid to be examined. This could be especially applicable for examining the viscosity of biological cells without damaging them. Laser trapping gives ability for measuring the inhomogeneous media, as it is possible to manipulate the trapped object in different directions and on short distances. Measuring cell viscosity of the biological cells is important for determining the state of the cells. The mechanical properties of the cells change corresponds to the intracellular changes. Sensing of the properties of the cells will develop new methods of treating cell diseases and understanding the cell transportation abilities.

We also applied the laser trapping for probing cell elasticity. The functions of cell are determined by the elasticity of cells, the sensing of which will help to understand the cell processes better. The fluorescent 500 nm polymer sphere was trapped close to the cell membrane. When the cell was indent by the polymer sphere, the displacement of the sphere was measured. Next, we compared the detected

displacements of the polymer sphere while indenting and not indenting the cell. Finally, we applied the Herts model for determining the cell elasticity.

As a further step, we plan to probe the cell elasticity all over the whole cell and to determine the elasticity difference depending on the place to be indent. In addition, we want to measure the cell elasticity changes when the foreign body is inverted into the cell. We plan to compare the elasticity of the live and sick, or even dead cells. Also after inverting the desired particle into the cell, we want to measure the viscosity of the cell by analyzing the displacements of the trapped manipulated particle.

Measuring the force applied by cell while transporting the particles inside of the cell is quite promising ability. It will provide a better understanding of the transportation inside of the cells, the knowledge about which will help in treating the cell diseases.

REFERENCES

[1] P. Lebedev Experimental examination of light pressure, Ann. der Physik (1901), 6, 433.

[2] A. Ashkin and J. Dziedzic, Optical levitation of liquid drops by radiation pressure, Science (1975) 187.

[3] A. Ashkin and J. Dziedzic, Optical trapping and manipulation of viruses and bacteria, Science (1987), Vol. 235, pp. 1517-1520.

[4] A. Ashkin, The study of cells by optical trapping and manipulation of living cells using infrared laser beams, ASGSB Bulletin (1991) 4(2).

[5] Steven Chu, J. Bjorkholm, A. Ashkin, and A. Cable, Experimental Observation of Optically Trapped Atoms, Physical review letters (1986), Volume 57, No. 3.

[6] K. Svoboda and Steven M. Block, Optical trapping of metallic Rayleigh particles, Opt. Lett.19 (1994), pp. 930-932.

[7] P. Bendix, L. Jauffred, K. Norregaard, and L. Oddershede, Optical Trapping of Nanoparticles and Quantum Dots, IEEE Journal OF Selected Topics in Quantum Electronics (2014), Vol. 20, No. 3.

[8] T. Iida and H. Ishihara, Theoretical study of the optical manipulation of semiconductor nanoparticles under an excitonic resonance condition, Phys. Rev. Lett. (2003), vol. 90, 057403-1–057403-4.

[9] J. Rodriguez-Fernandez, J. Perez-Juste, F. J. Garcia de Abajo, and L. M. Liz-Marzan, Seeded growth of submicron Au colloids with quadrupole plasmon resonance modes, Langmuir (2006), vol. 22, pp. 7007–7010.

[10] A. Rohrbach, Stiffness of Optical Traps: Quantitative Agreement between Experiment and Electromagnetic Theory, PRL (2005) 95, 168102.

[11] S. Reihani and L. Oddershede, Optimizing immersion media refractive index improves optical trapping by compensating spherical aberrations, Opt. Lett. (2007), vol. 32, pp. 1998–2000.

[12] F. Hajizadeh and S. Reihani, Optimized optical trapping of gold nanoparticles, Opt. Exp. (2010), vol. 18, pp. 551–559.

[13] Christine Selhuber-Unkel, Inga Zins, Olaf Schubert, and Carsten Sonnichsen, Lene B. Oddershede, Quantitative Optical Trapping of Single Gold Nanorods, Nano letters (2008), Vol. 8, No. 9, pp. 2998-3003.

[14] Jauffred L, Richardson AC,Oddershede LB, Three-dimensional optical control of individual quantum dots, Nano Lett. (2008), 8 (10), pp. 3376-80.
[15] Liselotte Jauffred, and Lene B. Oddershede Two-Photon Quantum Dot Excitation during Optical Trapping, Nano Lett. 2010, *10*, pp. 1927–1930.
[16] P.H. Jones, E. Stride and N. Saffari, Trapping and manipulation of microscopic bubbles with a scanning optical tweezer, Applied physics letters (2006) 89, 081113.
[17] Changan Xie, Mumtaz A. Dinno, and Yong-qing Li, Near-infrared Raman spectroscopy of single optically trapped biological cells, Optics letters (2002), Vol.27, No. 4, pp. 249-251.
[18] Changan Xie, Mumtaz A. Dinno, and Yong-qing Li, Near-infrared Raman spectroscopy of single optically trapped biological cells, Optics letters (2002), Vol. 27, No.4, pp. 249-251.
[19] Z. Kang, J. Chen, S. Wu, K. Chen, S. Kong, K. Yong, Ho-Pui Ho, Trapping and assembling of particles and live cells on large-scale random goldnano-island substrates, Scientific reports (2015) 5: 9978, pp. 1-8.
[20] I. Heller, G. Sitters, O. Broekmans, G. Farge, C. Menges, W. Wende, S. Hell, E. Peterman & G. Wuite, STED nanoscopy combined with optical tweezers reveals protein dynamics on densely covered DNA, Nature Methods (2013) 10, pp. 910-916.
[21] K. Neuman and S. Block, Optical trapping, Review of scientific instruments (2004), Vol. 75, No. 9, pp. 2787-2809.
[22] A. Radenovic, Optical trapping, advanced bioengineering methods laboratory optical trapping.
[23] A. Ashkin, Forces of a Single-Beam Gradient Laser Trap on a Dielectric Sphere in the Ray Optics Regime, Biophys. J. (1992), 61 (2), pp. 569–582.
[24] W. Wright, G. Sonek, Y. Tadir, and M. Berns, Laser trapping in cell biology. IEEE (Inst. Electr. Electron. Eng.) J. Quant. Elect. (1990) 26: 2148-2157.
[25] A. Ashkin, The study of the cells by optical trapping and manipulation of living cells using infrared laser beams, ASGSB Bullein (1991) 4(2): 133-146.
[26] Thorlabs, Large Beam Diameter Scanning Galvo Systems User Guide Original Instructions.
[27] Instructions Reflected Fluorescence System, http://sydney.edu.au/medicine/bosch/facilities/molecular-biology/digital-imaging/CKX-RFA.pdf

[28] K. Neuman, S. Block, Optical trapping, Rev. Sci. Instrum. (2004), Vol. 75(9) pp. 2787-2809.

[29] N. Osterman, TweezPAl – Optical tweezers analysis and calibration software, Computer Physics Communications 181 (2010) pp. 1911-1916.

[30] C. Xie, M.A. Dinno, Y.Q. Li, Y. Q, Near-infrared Raman spectroscopy of single optically trapped biological cells, Opt. Lett. 27 (2002) pp. 249–251.

[31] F. Zheng, Y. Qin, K. Chen, Sensitivity map of laser tweezers Raman spectroscopy for single-cell analysis of colorectal cancer, J. Biomed. Opt. 12 (2007) 034002.

[32] A. Rohrbach, C. Christian, D. Neumayer, E.L. Florin, E.H.K Stelzer, Trapping and tracking a local probe with a photonic force microscope, Rev. Sci. Instrumen. 75 (2004) pp. 2197–2210.

[33] S. Chu, J. Bjorkholm, A. Ashkin, A. Cable, Experimental Observation of Optically Trapped Atoms, Phys. Rev. Lett., 57 (3) (1986) pp. 314-317.

[34] K. Svoboda, S. Block, Optical trapping of metallic Rayleigh particles, Opt. Lett. 19, (1994) pp.930-932.

[35] P. Bendix, L. Jauffret, K. Norregaard, L.B. Oddershede, Optical Trapping of Nanoparticles and Quantum Dots, IEEE Journal of Selected Topics in Quantum Electronics 20 (3) (2014), pp. 15-26.

[36] L. Jauffred, A. C. Richardson, L.B. Oddershede, Three-dimensional optical control of individual quantum dots, Nano Lett. 8 (10) (2008) pp. 3376–3380.

[37] P. Jones, E. Stride, N. Saffari, Trapping and manipulation of microscopic bubbles with a scanning optical tweezer, Appl. Phys. Lett. 89 (2006) pp. 081113, 1-4.

[38] S. Ishizaka, K. Yamauchi, N. Kitamura, In situ Quantification of ammonium sulfate in single aerosol droplets by means of laser trapping and Raman spectroscopy, Analytical Sciences, Vol. 29 (2013) pp. 1223-1226.

[39] K. Ramser, D. Hanstorp, Optical manipulation for single-cell studies, J. Biophotonics 3 (2010) pp. 187-206.

[40] Y. Yang, Y. Shi, L. Chin, J. Zhang, D. Tsai and A. Q. Liu, Optofluidic nanoparticles sorting by hydrodynamic optical force**,** *2013 Transducers & Eurosensors XXVII: The 17th International Conference on Solid-State Sensors, Actuators and Microsystems (TRANSDUCERS & EUROSENSORS XXVII)***,** Barcelona (2013) 2122-2125.

[41] P. Zhang, D. Hernandez, D. Cannan, Y. Hu, S. Fardad, S. Huang, J. Chen, D. Christodoulides andZ. Chen, Trapping and rotating microparticles and bacteria with moiré-based optical propelling beams, Biomed. Opt. Express 3 (2012) 1891–1897.
[13] A.S Bezryadina, D.C Preece, J.C. Chen, Z. Chen, Optical disassembly of cellular clusters by tunable 'tug-of-war' tweezers, Light: Science & Applications (2016) 5, e16158.
[42] A.S Bezryadina, D.C Preece, J.C. Chen, Z. Chen, Optical disassembly of cellular clusters by tunable 'tug-of-war' tweezers, Light: Science & Applications (2016) 5, e16158.
[43] K. Lee, M. Kinnunen, M.D. Khokhlova, E.V. Lyubin, A.V. Priezzhev, I. Meglinski, A.A. Fedyanin, Optical tweezers study of red blood cell aggregation and disaggregation in plasma and protein solutions, Journal of Biomedical Optics, Vol. 21(3) (2016) 035001.
[44] I. Heller, G. Sitters, O.D. Broekmans, G. Farge, C. Menges, W. Wende, S.W. Hell, E.J.G. Peterman, G.J.L. Wuite, STED nanoscopy combined with optical tweezers reveals protein dynamics on densely covered DNA, Nature methods (2013) pp. 910-916.
[45] M. Yevnin, D. Kasimov, Y. Gluckman1, Y. Ebenstein, Y. Roichman, Independent and simultaneous three-dimensional optical trapping and imaging, Biomed. Opt. Express 4 (2013) pp. 2087-2094.
[46] Molecular Rotor Measures Viscosity of Live Cells via Fluorescence Lifetime Imaging, Marina K. Kuimova, Gokhan Yahioglu, James A. Levitt and Klaus Suhling, J. AM. CHEM. SOC. 130 (2008) pp. 6672–6673.
[47] I. Krasnikov, A. Seteikin, I. Bernhardt, Thermal processes in red blood cells exposed to infrared laser tweezers (λ= 1064 nm), J. Biophotonics 4, No. 3 (2011) pp. 206–212.
[48] K. Svoboda, S.M. Block, Biological applications of optical forces, Annu. Rev. Biophys. Biomol. Stmct. (1994) 23:247-85.
[49] B. Yameen, W.I. Choi, C. Vilos, A. Swami, J. Shi, O.C. Farokhzad, Insight into nanoparticle cellular uptake and intracellular targeting, Journal of Controlled Release 190 (2014) 485–499.
[50] S. Kanno, A. Furuyama, and S. Hirano, A murine scavenger receptor MARCO recognizes polystyrene nanoparticles, TOXICOLOGICAL SCIENCES 97(2) (2007) pp. 398–406.

[51] CISMM at UNC-CH, supported by the NIH NIBIB (NIH 5-P41-RR02170).
[52] Glycerine Producer's association, Physical properties of Glycerine and it's Solutions, Glycerine Producer's association, 1963.
[53] S. Bicknese, N. Periasamy, S. Shohet, and A. Verkman, Cytoplasmic Viscosity Near the Cell Plasma Membrane: Measurement by Evanescent Field Frequency-Domain Microfluorimetry Biophysical Journal (1993) Volume 65 September pp. 1272-1282.
[54] Comparative Analysis of Viscosity of Complex Liquids and Cytoplasm of Mammalian Cells at the Nanoscale, Tomasz Kalwarczyk, Natalia Zie-bacz, Anna Bielejewska, Ewa Zaboklicka, Kaloian Koynov, Je-drzej Szymanski, Agnieszka Wilk, Adam Patkowski, Jacek Gapiński, Hans-Jürgen Butt, and Robert Hołyst, Nano Lett. (2011) 11, pp. 2157–2163.
[55] D. Haussinger, The role of cellular hydration in the regulation of cell function, Biochem. J. (1996) 313, pp. 697–710.
[56] N. R. Patel, M. Bole, C. Chen, C.C. Hardin, A.T. Kho, J. Mih, L. Deng, J. Butler, D. Tschumperlin, J.J. Fredberg, R. Krishnan, H. Koziel, Cell Elasticity Determines Macrophage Function. PLoS ONE (2012) 7(9): e41024.
[57] N. R. Patel, M. Bole, C. Chen, C.C. Hardin, A.T. Kho, J. Mih, L. Deng, J. Butler, D. Tschumperlin, J.J. Fredberg, R. Krishnan, H. Koziel, Cell Elasticity Determines Macrophage Function. PLoS ONE (2012) 7(9): e41024.
[58] S. Safrana, N. Govb, A. Nicolasc, U. Schwarzd, T. Tlustya, Physics of cell elasticity, shape and adhesion, Physica A 352 (2005) pp. 171–201.
[59] D. Lin, I. Shreiber, E. Dimitriadis, F. Horkay, Spherical indentation of soft matter beyond the Hertzian regime: numerical and experimental validation of hyperelastic models, Biomech Model Mechanobiol. (2009), 8(5), pp. 345–358.
[60] Tatyana G. Kuznetsova, Maria N. Starodubtseva, Nicolai I. Yegorenkov, Sergey A. Chizhik, Renat I. Zhdanov, Atomic force microscopy probing of cell elasticity, Micron 38 (2007) pp. 824–833.
[61] S. Nawaz, P. Sanchez, K. Bodensiek, S. Li, M. Simons, I. Schaap, Cell visco-elasticity measured with AFM and Optical Trapping at Sub-Micrometer Deformations, PloS ONE (2012) Vol. 7 (9), e45297, pp. 1-9.